DEUTSCHES ELEKTRONEN-SYNCHROTRON DESY

DESY 81-071
October 1981

RECENT e^+e^- RESULTS FROM PETRA

by

Sau Lan Wu

Department of Physics, University of Wisconsin
Madison, Wisconsin, USA
and
Deutsches Elektronen-Synchrotron DESY, Hamburg

NOTKESTRASSE 85 · 2 HAMBURG 52

To be sure that your preprints are promptly included in the
HIGH ENERGY PHYSICS INDEX ,
send them to the following address (if possible by air mail) :

DESY
Bibliothek
Notkestrasse 85
2 Hamburg 52
Germany

DESY 81-071
October 1981

RECENT e^+e^- RESULTS FROM PETRA *

by

Sau Lan Wu

Department of Physics, University of Wisconsin, Madison, Wisconsin, USA +

and

Deutsches Elektronen Synchrotron DESY, Hamburg, Germany.

Abstract

Recent experimental data are reviewed from the five detectors at PETRA: CELLO, JADE, MARK J, PLUTO, and TASSO. The many interesting new results include, for example, the copious production of baryons, especially Λ and $\bar{\Lambda}$, and the observation of forward-backward asymmetry for $e^+e^- \to \mu^+\mu^-$ due to weak and electromagnetic interference. Some future plans at PETRA are also discussed.

* Rapporteur talk at the Topical Conference of the 1981 SLAC Summer Institute on Particle Physics, July 27 - August 7, 1981, SLAC, Stanford, California, USA.

+ Supported by the US Department of Energy, Contract EY-76-C-02-0881.

1. INTRODUCTION

At present there are five detectors at PETRA: CELLO, JADE, MARK J, PLUTO and TASSO. All five detectors have been operating well, and four of them - CELLO, JADE, MARK J. and TASSO - are taking data at present. The fifth one, PLUTO, will be moved into the beam for the second time in September 1981, equipped with a new forward detector specially built for two-photon physics. There is therefore a great deal of recent data to be reported here, and it is necessary to be brief on each piece of new data. The topics to be covered are:

1. PETRA Status,
2. Baryon Production,
3. Lifetimes of the τ and Bottom Meson,
4. Jet Analysis,
5. Properties of the Gluon,
6. Two-Photon Physics,
7. Electroweak Interaction.

Since results from PEP are given in this proceedings by J.Dorfan, no results from PEP will be given in this paper.

2. PETRA STATUS

PETRA (Positron-Electron Tandem Ring Accelerator) has been operating for nearly three years and performing very well. The most recent improvement was the addition, in March 1981, of focusing quadrupole magnets in so called "mini-beta" sections [1]. This name is derived from the purpose of these quadrupoles to reduce the beta values at the intersection points, because luminosity is inversely proportional to the geometric mean of the horizontal and vertical beta values. Steffen [2] first pointed out how this reduction of β can actually be accomplished at PETRA, and by now the experimental increase in luminosity is in accurate agreement with this theoretical evaluation.

The β values are shown in Table 1, for pre-mini-beta, the present mini-beta scheme, and also a proposed future mini-beta II by Steffen, Voss and Wolf [3]. Theoretical increases in luminosity partially based on the formula luminosity α $(\beta_{vertical}\ \beta_{horizontal})^{-1/2}$ are also shown. The increase in luminosity (nb^{-1} per day) is plotted in Fig. 1 for the period of March and April 1981 when the mini-beta scheme was working for the first time at PETRA. So far the best luminosities are as follows:

luminosity = 1.7×10^{31} cm^{-2} sec^{-1}

integrated luminosity = $\begin{matrix} 790\ nb^{-1}/day\ \text{(PETRA ungated)} \\ 600\ nb^{-1}/day\ \text{(TASSO gated)} \end{matrix}$

Table 1 - Mini-beta schemes and increases in luminosity

	Pre-mini-beta	Mini-beta	Mini-beta II
$\beta_{vertical}$ (cm)	20	8	1.14
$\beta_{horizontal}$ (cm)	190	120	51
Luminosity ratio	1	3 *	11 *

One of the major problems that had to be solved before the success of the present mini-beta scheme is the reduction of the distance between the interaction point to the nearest quadrupoles. This reduction from 7.5 m to the present 4.45 m is achieved by eliminating the compensating magnets in TASSO and JADE. This is possible because TASSO and JADE can compensate each other.

In mini-beta II [3], the beta values are further reduced to obtain another increase in luminosity of almost a factor of 4. In this

* These numbers include the additional improvement due to better control of orbit, vertical dispersion and ring symmetry which gives smaller vertical beam sizes.

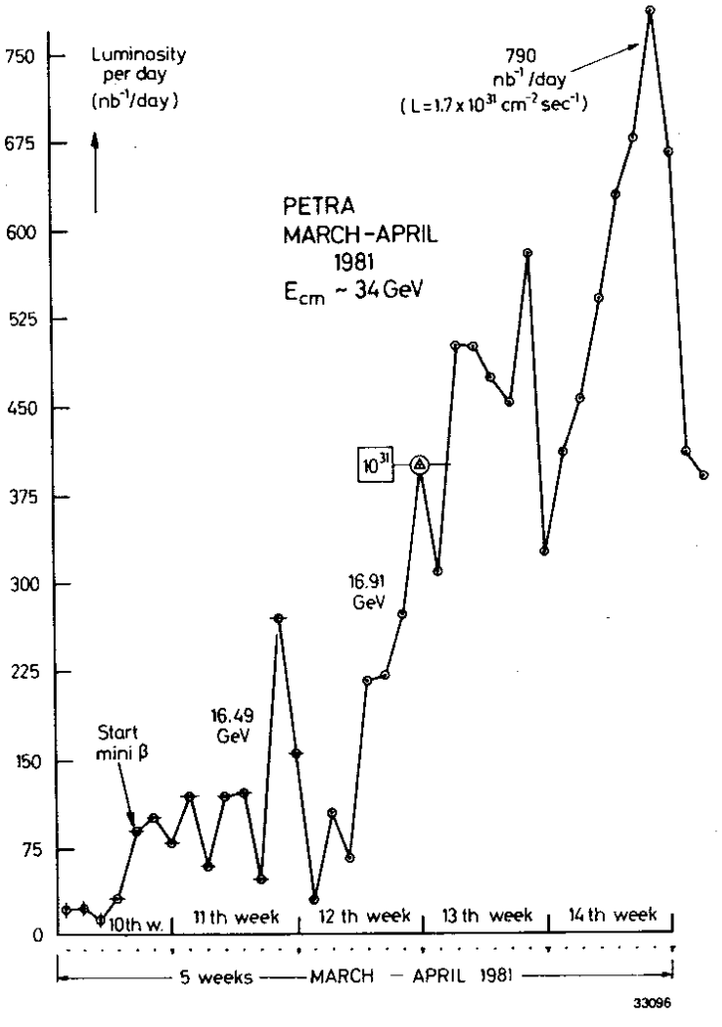

Fig. 1 - Luminosity per day at PETRA during the four weeks period after the start of mini β.

proposed scheme, iron-free superconducting quadrupoles similar to the Fermilab design are used: they are 1.7 m long, 4 cm aperture radius, and 10 cm outer radius, and are placed $\sim$ 1 m away from the interaction point. A major problem for this future design is to allow space for small-angle luminosity monitors and two-photon forward detectors. The scheme is shown [3] in Figure 2, and the target date for its installation is the end of 1982 or early 1983.

The other major future improvement for PETRA is the increase in energy which is underway. It is planned to double the rf power from 4 MW to 8 MW in the spring of 1982 so that the total center-of-mass energy $\sqrt{s}$ is increased from the present 36.7 GeV to about 41 GeV. In 1983, it is further planned to install additional rf cavities in the remaining two straight sections so that $\sqrt{s}$ is increased to 45 GeV. The plan after 1983 is less certain: the general plan is to reach even higher energies by using superconducting rf cavities.

3. BARYON PRODUCTION - TASSO, JADE

One of the recent excitements at PETRA is the observation of the copious production of baryons. About a year ago, TASSO observed the inclusive production of protons and antiprotons [4]. More recently, JADE [5] confirmed the inclusive antiproton spectrum to about 1 GeV/c and also observed the inclusive anti-Λ spectrum to about 1.4 GeV/c, while TASSO [6] obtained the Λ and $\bar{\Lambda}$ spectrum all the way up 10 GeV/c in momentum.

In JADE, $\bar{p}$ is identified by dE/dx in the drift chamber, while $\bar{\Lambda}$ is identified through the decay mode $\bar{\Lambda} \to \bar{p}\,\pi^+$. To discriminate against $K_s \to \pi^+\pi^-$, the momentum of the π^+ is required to be less than 40% of the momentum of the $\bar{p}$. In the invariant mass plot, the $\bar{\Lambda}$ peak is seen very clearly. In TASSO, the p and $\bar{p}$ are identified by time-of-flight,

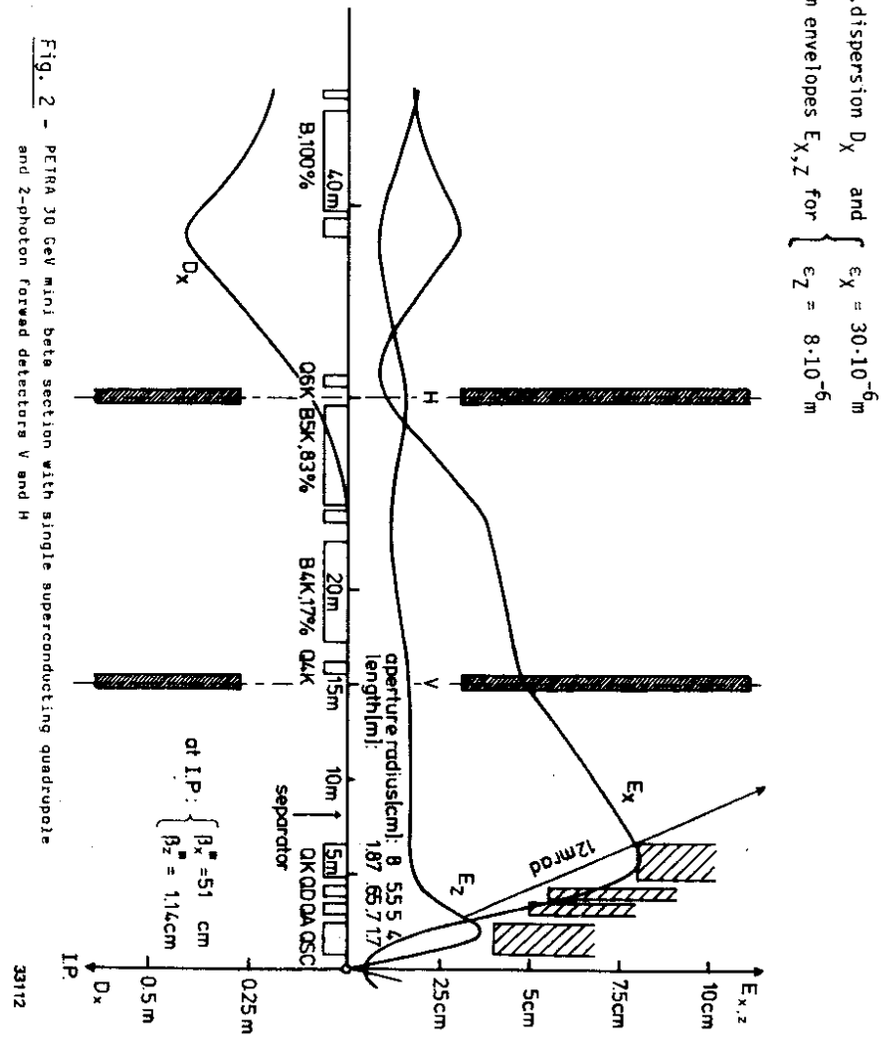

Fig. 2 - PETRA 30 GeV mini beta section with single superconducting quadrupole and 2-photon forward detectors V and H

while the Λ and $\bar{\Lambda}$ are identified by vertex fits to oppositely charged pairs, where the higher-momentum particle is taken to be the p or $\bar{p}$. Two different methods [6] of analysis are used for Λ and $\bar{\Lambda}$, with method 1 emphasizing the lower momentum Λ and $\bar{\Lambda}$ and method 2 the higher momenta ones. Invariant mass plots from method 1 are shown in Fig. 3. The experimental results from both TASSO and JADE are summarized in Fig. 4 together with a comparison with the K^0 yield.

In Table 2, the results of JADE and TASSO are compared. While the results on $\bar{p}$ are barely compatible, those on $\bar{\Lambda}$ are in some disagreement. This may be due to the extrapolation procedure used by JADE. For the extrapolation of $\bar{p}$ and $\bar{\Lambda}$ to all momenta the shape predicted by the LUND model [7] has been used by JADE. Note that the observed p and $\bar{p}$ include those due to the decay of Λ and $\bar{\Lambda}$. Another way to express the TASSO results on Λ and $\bar{\Lambda}$ is.

$$R_{\Lambda+\bar{\Lambda}} = \frac{\sigma(e^+e^- \to \Lambda x) + \sigma(e^+e^- \to \bar{\Lambda} x)}{\sigma(e^+e^- \to \mu^+\mu^-)} = 1.12 \pm 0.15 \pm 0.17$$

where as usual the first error is statistical while the second one is systematic. Here extrapolation has been carried out to cover also the unobserved range of 0 - 1 GeV/c, which contributes 13% of this value. In this extrapolation, a form of $a \cdot \exp(-bE)$ is used in parameterising the invariant cross section $(E/4\pi p^2)\, d\sigma/dp$ over the momentum range from 1 to 5 GeV/c.

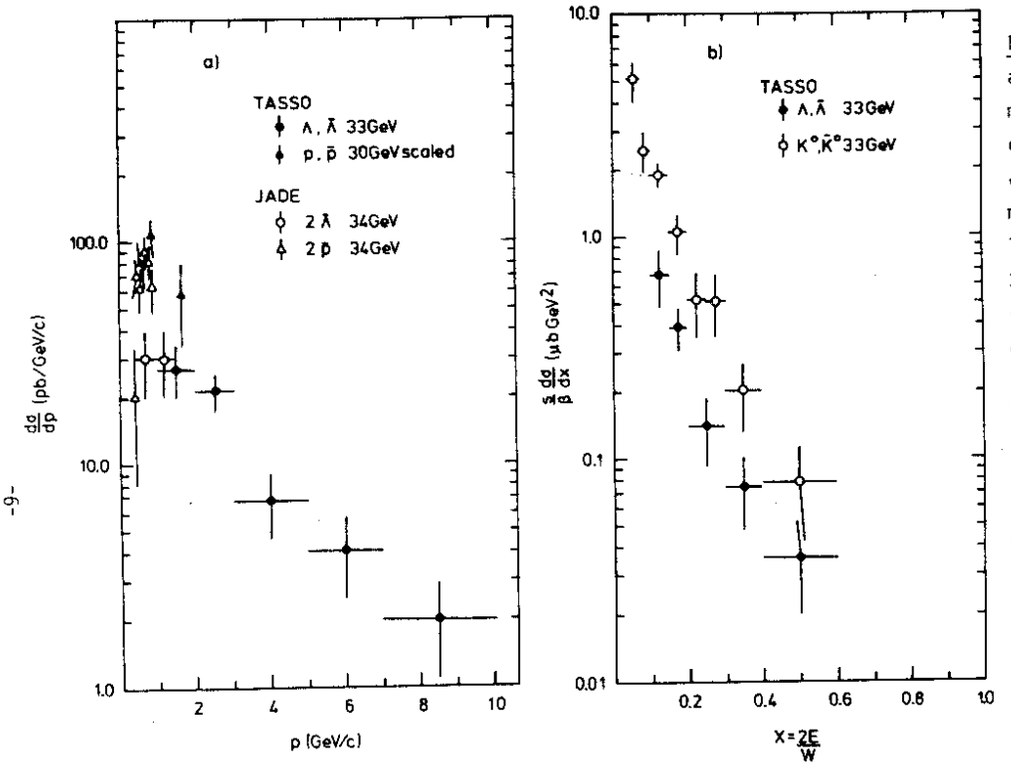

Fig. 4

a) TASSO results on differential momentum cross section for the sum of Λ, $\bar{\Lambda}$ production. Also shown are JADE results on $\bar{\Lambda}$ and $\bar{p}$ production multiplied by a factor of two and TASSO results on p, $\bar{p}$ production at 30 GeV. The 30 GeV points have been scaled with s^{-1} to the mean energy of 33.3 GeV.

b) TASSO results on scaling cross section $(s/\beta)\, d\sigma/dx$ for the sum of Λ, $\bar{\Lambda}$ production. Also shown are the K^0 data at 33.3 GeV centre of mass energy from TASSO.

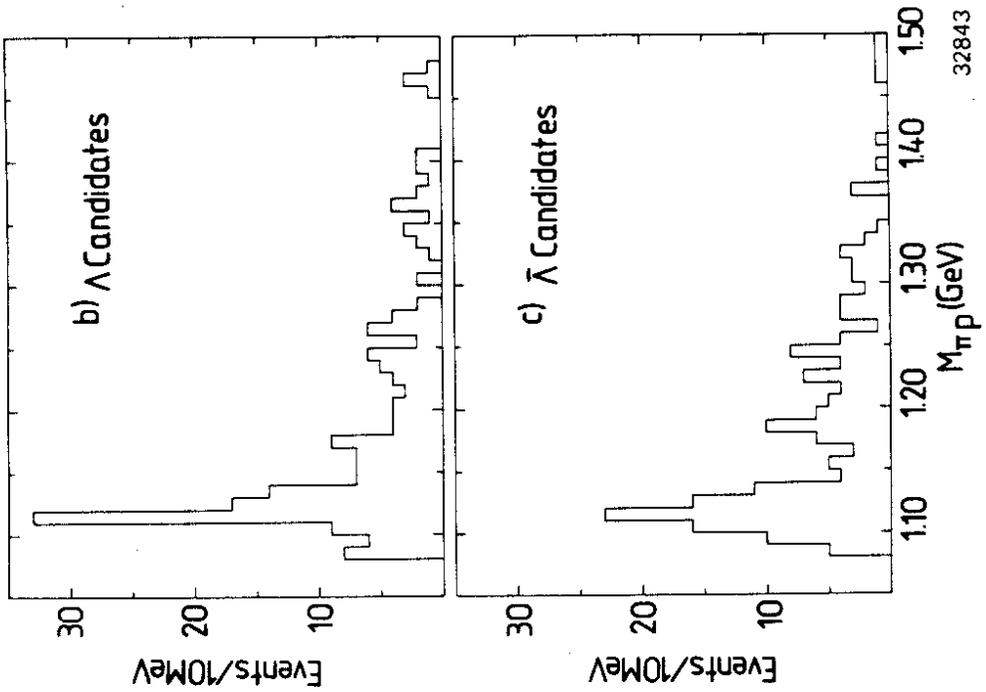

Fig. 3 - a) $M_{p\pi^-}$ spectrum for Λ candidates
b) $M_{\bar{p}\pi^+}$ spectrum for $\bar{\Lambda}$ candidates.
Results from TASSO

Table 2 - Baryon production at PETRA

a) JADE results [5] for c.m. energy between 30 and 36 GeV

Particle type	momentum range	average number of particle per hadron event
$\bar{p}$	0.3 - 0.9 GeV/c (observed)	0.062 ± 0.006
$\bar{p}$	all momenta (extrapolated)	0.27 ± 0.03
$\bar{\Lambda}$	0.4 - 1.4 GeV/c (observed)	0.037 ± 0.010
$\bar{\Lambda}$	all momenta (extrapolated)	0.117 ± 0.032

b) TASSO results [4,6] for c.m. energy between 30 and 36 GeV

Particle type	momentum range	average number of particle per hadronic event
$p + \bar{p}$	0.5 - 2.2 GeV/c (observed)	at least 0.4
$\Lambda + \bar{\Lambda}$	1 - 10 GeV/c (observed)	$0.24 \pm 0.04 \pm 0.04$
	all momenta (extrapolated)	$0.28 \pm 0.04 \pm 0.04$ -

How are the baryons formed ? Until recently, the popular models of hadron production in electron-positron annihilation did not include baryons at all [8-13]. The reason is that it takes three quarks to form a baryon, and this has been considered to be difficult. Another way of saying this is that the color tube has to double back on itself in order to bring three quarks together. Since the observation of baryons at PETRA, there have been several attempts to include baryons in the previously developed models. In both cases, diquarks are introduced as entities distinct from quarks. In the LUND version [7], it is assumed that diquark pairs are produced by the color force field in addition to quark pairs with a relatively low probability

$$\frac{P(qq)}{P(q)} = 0.065 .$$

This ratio was extracted from SPEAR data [14,15] in the 4 GeV center of mass region. In the version of Meyer [16], the Field-Feynman scheme [9] (Fig. 5(a)) is used to include diquark pairs with a similar probability

$$P_{B1} = \frac{P(qq)}{P(q) + P(qq)} = 0.075$$

based on TASSO data [4]. This is shown schematically in Fig. 5(b). The ratios of u, d and s quark pairs are taken as before at 2 : 2 : 1, and the ratio of diquark pairs are taken similarly. The results of these two procedures are shown in Fig. 6. For the solid curve of Meyer in this figure, a second mechanism for diquark pair production has been added as shown in Fig. 5(c). The data are not sensitive enough to support this second mechanism, which in the simplest form tends to increase e^+e^- total hadronic cross section in contradiction with other data [17].

Although the Meyer results agree better with experimental data than the LUND results, a far more interesting and profound point is that these two models produce Λ and $\bar{\Lambda}$ in two qualitatively different ways. In the LUND version, cascades (Ξ^0 and Ξ^-) are hardly produced while the decay $\Sigma^0 \to \Lambda\gamma$ is an important source of Λ. In the Meyer version, the opposite is true: $\Sigma^0 \to \Lambda\gamma$ contributes no more than 20% of the Λ's, while the production of Ξ^0 and Ξ^- is significant. In this way the two models can be distinguished.

We list some of the problems that can perhaps be studied in the near future in connection with baryon production in e^+e^- annihilation.

(i) Short-range baryon-antibaryon correlation. This is universally expected on the basis of most models, and JADE has some preliminary information on this issue [5].

(ii) Long-range baryon-antibaryon correlation.

(iii) Polarization of Λ and $\bar{\Lambda}$. This would give us some information about the source of the Λ's. For example, are Λ's mainly coming from decay of Λ_c's ?

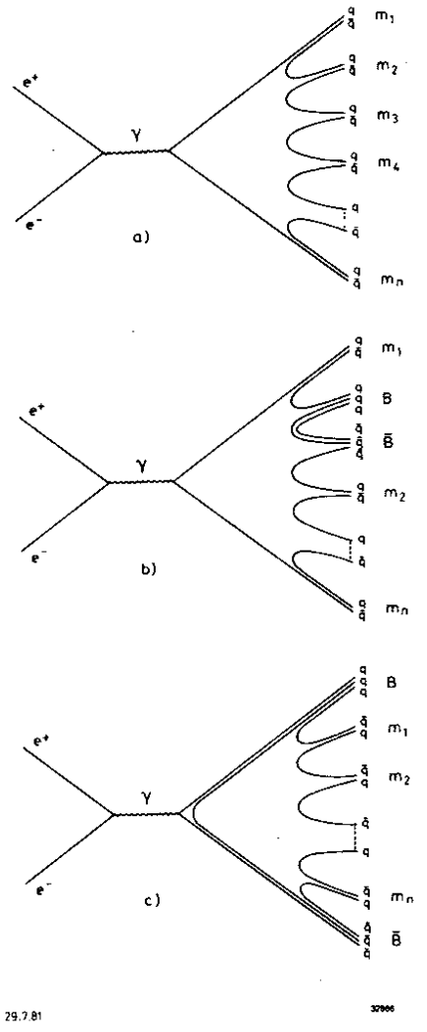

Fig. 5 - a) Diagram for e^+e^- → mesons
b) Diagram for e^+e^- → mesons and baryons
c) Diagram for e^+e^- → mesons and baryons with leading baryons in each jet.

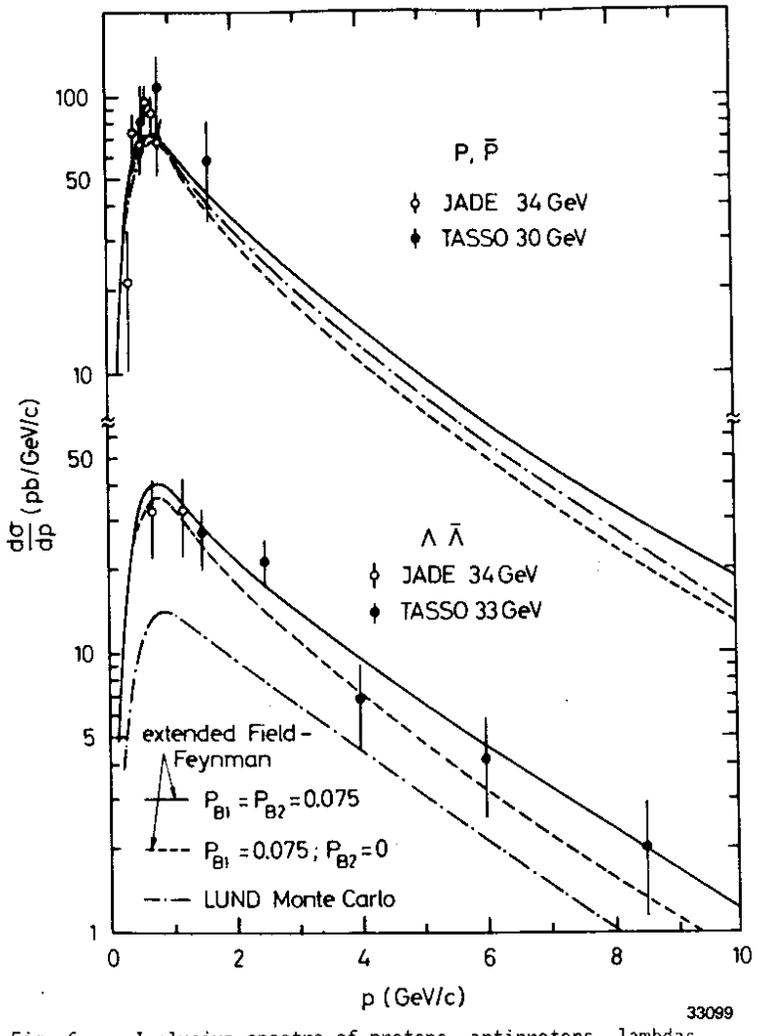

Fig. 6 - Inclusive spectra of protons, antiprotons, lambdas, and antilambdas. Data by the TASSO [4, 6] and the JADE[5] Collaborations. (All data points have been scaled with s^{-1} to the energy of 33 GeV).
Solid curves: $P_{B1} = P_{B2} = 0.075$
Dashed curves: $P_{B1} = 0.075$, $P_{B2} = 0.$ } Meyer [16]
Dashed dotted-dashed curve: LUND Model [7] .

(iv) Production of Σ^0 and $\bar{\Sigma}^0$.

(v) Production of Ξ and $\bar{\Xi}$.

Let us summarize the present status of knowledge about baryon production at PETRA.

(1) Λ and $\bar{\Lambda}$ are copiously produced up to large momenta (10 GeV/c) and large x ($\sim$ 0.6) ($x = 2E/\sqrt{s}$).

(2) As a function of energy, the x-dependence of the scaling cross sections of baryons and kaons are similar, as shown in Fig. 4(b). This may be an indication that the production mechanisms of baryons and mesons are similar in high energy electron-positron annihilation.

(3) Comparing with SPEAR and DORIS data [15, 18-20] at $\sqrt{s}$ = 7 GeV, we concluded that the production of Λ increases more rapidly with energy than K^0, as shown in Table 3.

(4) The inclusive cross section for Λ and $\bar{\Lambda}$ are higher than those predicted by the LUND Model [7] but in reasonable agreement with the extended Field-Feynman Model of Meyer [16]. The number of Λ and $\bar{\Lambda}$ per event is 0.28, 0.13 and 0.3 for TASSO data [6], LUND and Meyer respectively.

Table 3 - Increase of Λ and K^0 production with energy

$\sqrt{s}$	7 GeV [18]	33 GeV [6,21]
$R_{\Lambda+\bar{\Lambda}} = \dfrac{\sigma(e^+e^- \to \Lambda x) + \sigma(e^+e^- \to \bar{\Lambda} x)}{\sigma(e^+e^- \to \mu^+\mu^-)}$	0.24 ± 0.02	$1.12 \pm 0.15 \pm 0.17$
$R_{K^0+\bar{K}^0} = \dfrac{\sigma(e^+e^- \to K^0 x) + \sigma(e^+e^- \to \bar{K}^0 x)}{\sigma(e^+e^- \to \mu^+\mu^-)}$	2.0 ± 0.2	$5.5 \pm 0.4 \pm 0.8$

4. LIFETIME OF THE τ AND BOTTOM MESON

A. New upper limit for τ lifetime - TASSO

Upper limits on the τ lifetime have previously been given by DELCO [22] and TASSO [23]. They are

$$\text{DELCO} : \tau_\tau < 2.3 \times 10^{-12} \text{ sec (95\% C.L.)}$$

$$\text{TASSO} : \tau_\tau < 1.4 \times 10^{-12} \text{ sec (95\% C.L.)}$$

The latter was based on approximately 3000 nb^{-1} of running at PETRA for $\sqrt{s}$ between 12 and 31.6 GeV.

A new upper limit was recently obtained as [24]

$$\text{TASSO} : \tau_\tau < 5.7 \times 10^{-13} \text{ sec (95\% C.L.)}$$

based on approximately 20,000 nb^{-1} of running for $\sqrt{s}$ between 27 GeV and 37 GeV.

These upper limits may be compared with the theoretical value obtained by scaling the μ lifetime and neglecting the electron mass:

$$\text{Theory} : \tau_\tau = BR(\tau \to e\, \nu\, \bar{\nu})(m_\mu/m_\tau)^5\, \tau_\mu$$
$$= (2.7 \pm 0.2) \times 10^{-13} \text{ sec},$$

where the error is due almost entirely to the uncertainty in the branching ratio $\tau \to e\, \nu\, \bar{\nu}$.

Recently, MARK II at PEP has obtained a measurement of the τ lifetime being $(4.6 \pm 1.9) \times 10^{-13}$ sec. This will be discussed in detail by Dorfan [25] in the next presentation.

Briefly, this new upper limit is obtained as follows. Consider events where there are three charged tracks on one side versus only one charged track on the other side such that the total charge is zero. With suitable cuts to reduce background due to radiative Bhabha scattering, there are 150 such events, one of which is shown in Fig. 7. From the side with three charged tracks the position of the τ decay vertex is determined in the

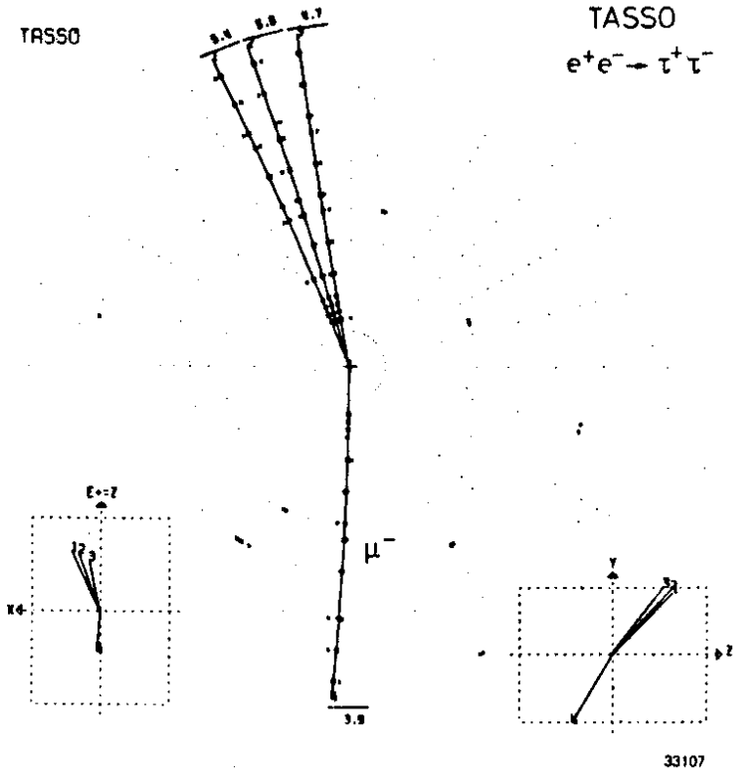

Fig. 7 - A $e^+e^- \to \tau^+\tau^-$ event from TASSO

transverse plane. The distribution of the resulting transverse distance to the interacting point is shown in Fig. 8. Using the polar angle of the momentum vector of each τ, this transverse distance is converted to a proper time, as shown in Fig. 8. The mean proper time of $(-0.25 \pm 3.5) \times 10^{-13}$ sec leads to the above mentioned upper limit of 5.7×10^{-13} sec at 95% confidence level.

B. New upper limit for the lifetime of botton meson - JADE

JADE [26] has recently obtained an interesting upper limit for the lifetime τ_B of the lightest meson with bottom quantum number. The events used are those hadronic events where there is a single muon with momentum larger than 1.8 GeV/c. There are 73 such events. From each of these events, the closest approach of the μ track to the interaction point is determined in the plane transverse to the e^+, e^- beam directions. Upper limit for this distance d_μ is found to be

$$d_\mu < 0.79 \text{ mm} \qquad (90\% \text{ C.L.})$$

This leads to an upper limit for τ_B

$$\tau_B < 5 \times 10^{-12} \text{ sec} \quad (90\% \text{ C.L.})$$

5. JET ANALYSIS

A. Long-range charge correlation - TASSO, JADE

Since two-jet events in electron-positron annihilation are due to the creation of $q\bar{q}$ pairs, and quarks are charged, it is to be expected that the leading particles in one jet "know" about the charge of the leading particles in the opposite jet. This long-range charge correlation was first observed by TASSO [27,28]. Let y be the rapidity variable defined by

$$y = \frac{1}{2} \ln \frac{E + p_\parallel}{E - p_\parallel}$$

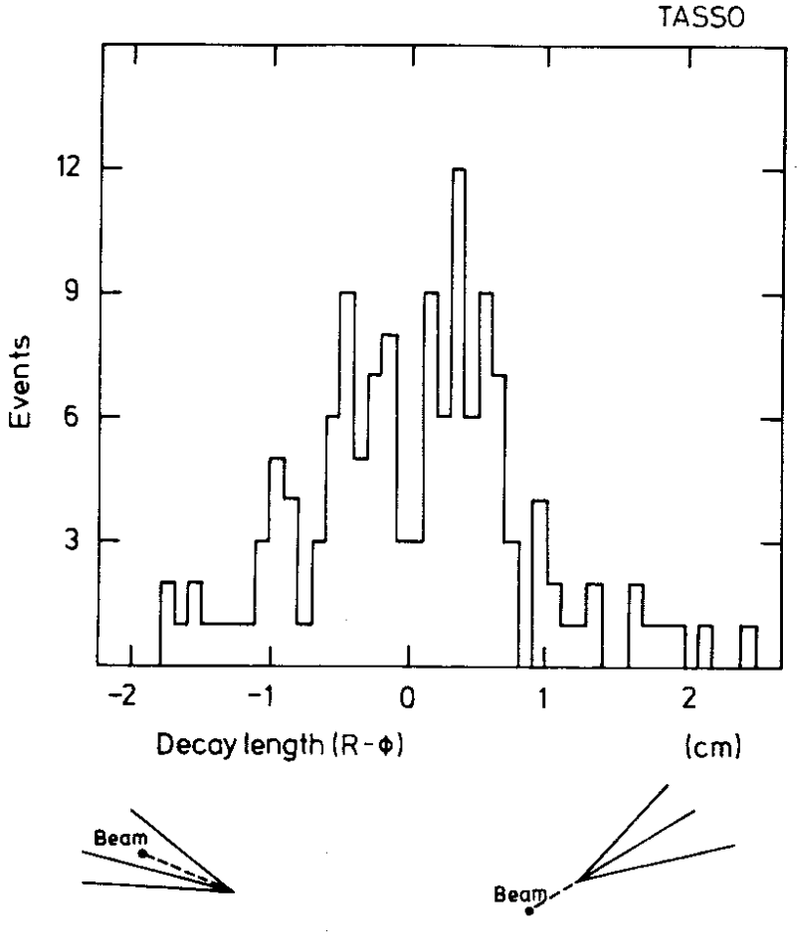

Fig. 8 - Distribution of decay lengths (distance from the fitted vertex position to the known beam position on the plane perpendicular to the e^+, e^- beam direction i.e. R-ϕ plane) from the tau decay candidates.

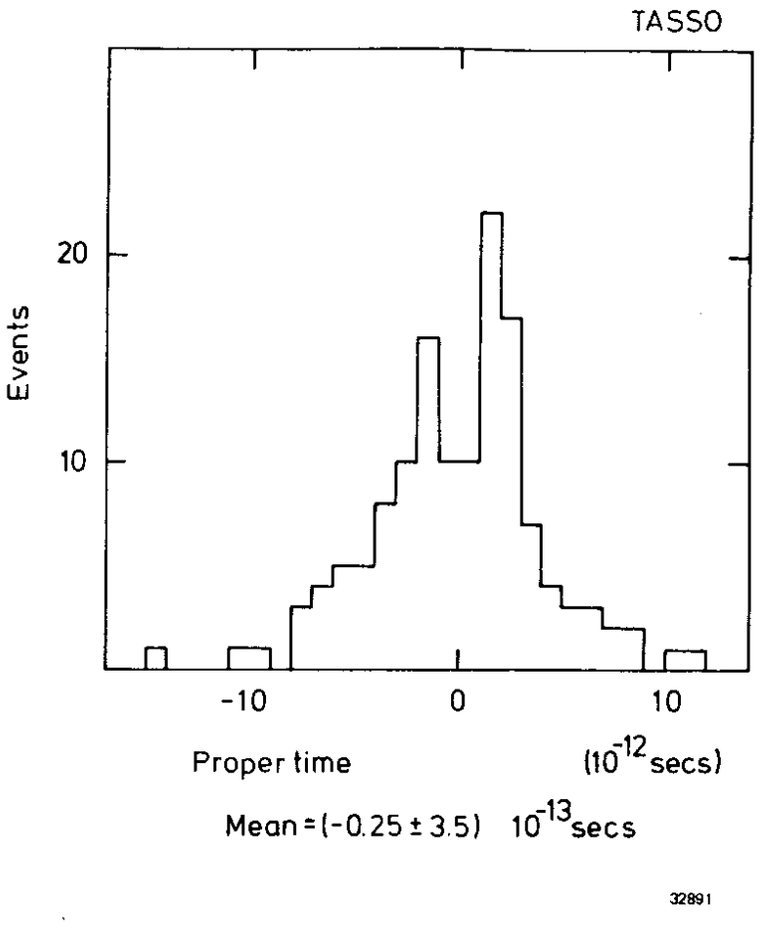

Fig. 9 - τ decay time distribution from TASSO.

for each observed track, where $p_{\parallel}$ is the component of the momentum parallel to the jet axis and the energy E is evaluated assuming the mass to be that of $\pi^{\pm}$. Define

$$\phi_r\,(y,y') = \frac{-1}{\Delta y \Delta y'} \left\langle \frac{1}{n} \sum_{k=1}^{n} \sum_{j\neq k}^{n} e_j\, \delta_{jy}\, e_k\, \delta_{ky'} \right\rangle$$

where e_j is the charge of the jth particle, n is the chargedmultiplicity of the event, and δ_{jy} is 1 if the jth particle is in the rapidity range Δy around y. Then the quantity

$$\overset{\sim}{\phi}_r\,(y,y') = \phi_r\,(y,y') \;/\; \int \phi_r\,(y,y')\,dy$$

can be interpreted as the probability for the charge of a particle produced at y' to be compensated at y. In Fig. 10 we show this $\overset{\sim}{\phi}_r(y,y')$ for four intervals of y':
(a) $-0.75 \leq y' \leq 0$; (b) $-1.5 \leq y' \leq -0.75$; (c) $-2.5 \leq y' \leq -1.5$; and (d) $-5.5 \leq y' \leq -2.5$. Short-range charge correlation is evident in all four cases, long-range charge correlation is clearly seen in (d).

Recently, this charge correlation analysis was repeated by JADE [29]. The new results are shown in Fig. 11 with only a slightly different choice of the ranges for y'. Again the long range charge correlation is clearly seen in case (d), where the y' range is $-5.5 \leq y' \leq -2.75$.

B. Neutral energy - JADE

Both JADE and CELLO can detect photons in 90% of the 4π solid angle, JADE with lead glass counters and CELLO with liquid argon counters. We report here the results from JADE [30].

Two energy fractions are defined as follows: the neutral energy fraction ρ_N is the fraction of energy not carried by charged particles

$$\rho_N = 1 - \sum_j E_j^{ch} \;/\; \sqrt{s}$$

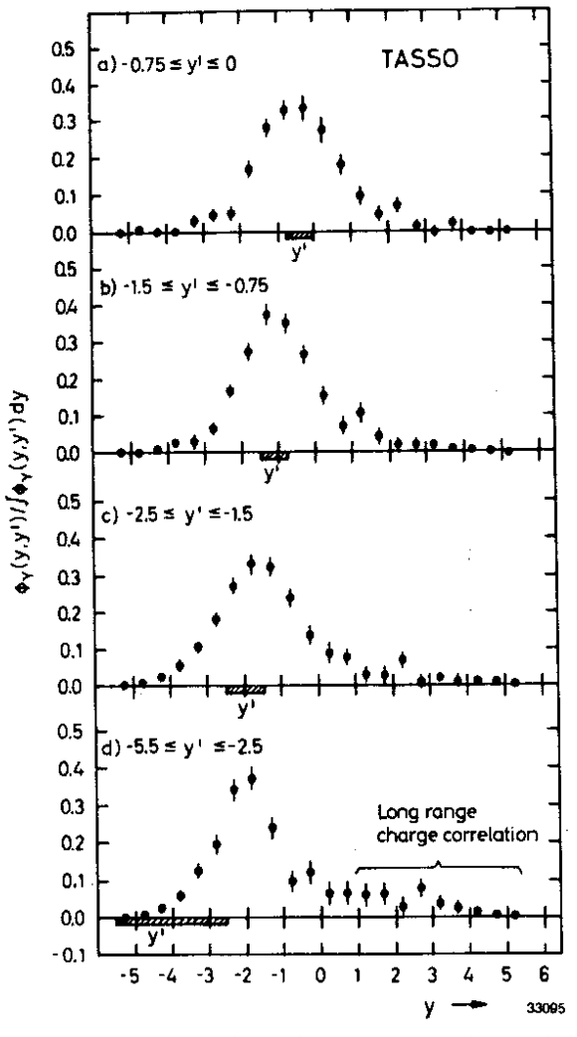

Fig. 10 - Results from TASSO on charge compensation probability $\phi_r(y,y') / \int \phi_r(y,y')\,dy$ as a function of rapidity y for a particle produced at y'.

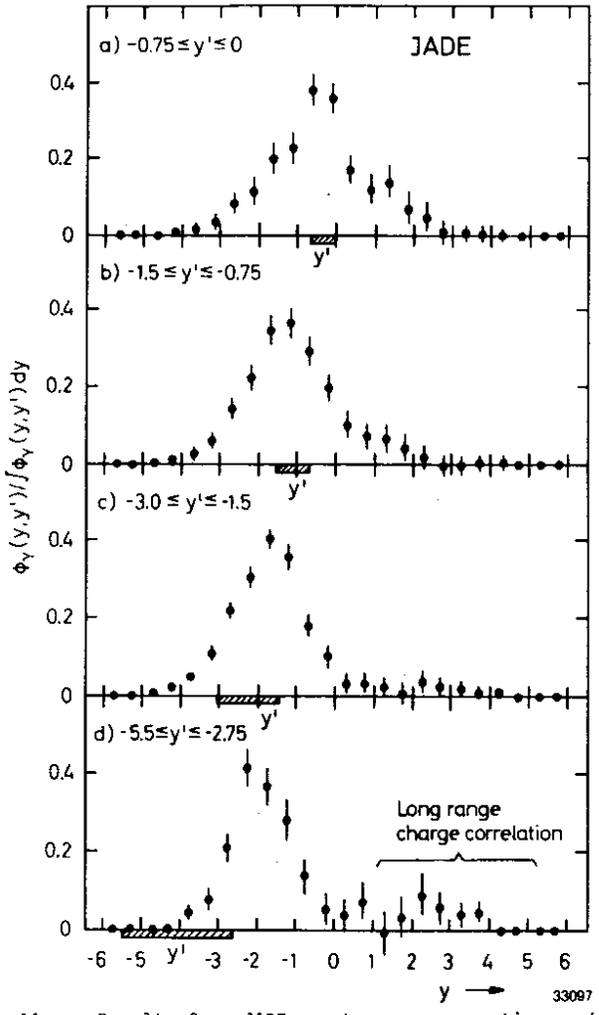

Fig. 11 - Results from JADE on charge conpensation probability $\phi_r(y,y')/\int\phi_r(y,y')\,dy$ as a function of rapidity y for a particle produced at y'.

and the photon fraction by

$$\rho_\gamma = \sum_j E_j^\gamma / \sqrt{s}.$$

The major contribution to ρ_γ is of course due to π^0. Both quantities have to be carefully corrected. For example, ρ_N includes contributions from K_s and Λ, while for ρ_γ the energy deposited in the lead glass counters by charged particles must be subtracted out.

The difference $\rho_N - \rho_\gamma$ is the fraction of energy carried by long-lived hadrons and neutrinos. The long-lived hadrons include K_L, n, and $\bar{n}$. Using available data at PETRA, these contributions can be estimated and in this way we obtain

ρ_ν = energy fraction carried by neutrinos.

The results are plotted in Fig. 12 and the corrected mean ρ_γ, ρ_N and ρ_ν are listed in Table 4. No difference is seen between two-jet events and planar events.

The most interesting feature of the result is that the fraction of energy carried by neutrinos is quite small. This excludes the Pati-Salam model [31], where multihadron final states arise via quarks of integer charge which decay into hadrons and neutrinos, giving rise to a neutrino energy fraction ρ_ν between 18% and 28%.

Table 4 - The corrected Gamma Ray, Neutral Particle and Neutrino Energy Fractions

$\sqrt{s}$ (GeV)		ρ_γ	ρ_N	Neutrino
12.00	All events	0.25 ± 0.04	0.37 ± 0.04	0.00 ± 0.06
	Planar	0.21 ± 0.05	0.32 ± 0.05	-0.01 ± 0.07
30.30	All events	0.28 ± 0.03	0.36 ± 0.04	-0.03 ± 0.05
	Planar	0.28 ± 0.03	0.36 ± 0.04	-0.03 ± 0.06
34.89	All events	0.30 ± 0.03	0.38 ± 0.04	-0.02 ± 0.05
	Planar	0.32 ± 0.03	0.41 ± 0.04	-0.02 ± 0.06

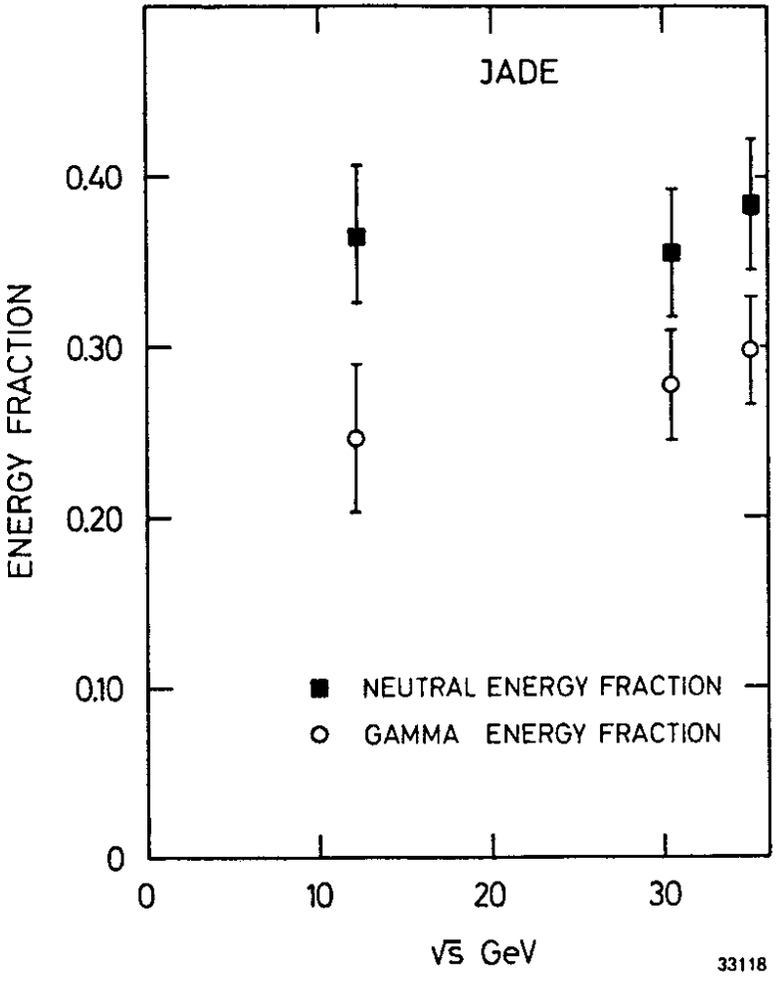

Fig. 12 - Results from JADE on the corrected mean gamma ray and neutral energy fractions versus center-of-mass energy.

C. Thrust and energy-flow distributions of photons - CELLO

In an attempt to find out whether neutral and charged particles are distributed similarly in electron-positron annihilation, CELLO obtained the thrust using separately the charged particles only and the photons only, which come mostly from π^0 decay. The result [32] is shown in Fig. 13, where the histograms represent the experimental data while the circles with error bars are obtained from a Monte Carlo simulation. It is seen that the thrust distribution is virtually identical for charged particles and for photons.

Continuing the comparison, CELLO next studied the energy flow distribution [33] which is for many purposesa more sensitive quantity. With an oblateness [34] cut of ≥ 0.15, the result is shown in Fig. 14. Again the energy flow pattern for photonsalone is the same as that for charged particles plus photons.

D. Energy flow distribution - MARK J

MARK J has compared their energy-flow pattern with a number of models. With an oblateness cut of > 0.3, the result [35] is shown in Fig. 15. As expected, the best agreement is obtained from QCD and the data disagree with models of $q\bar{q}$, phase space, and a $q\bar{q}$ model with a $\exp(-P_T/650\ \text{MeV})$ fragmentation distribution. This offers one more piece of evidence in favor of QCD. We shall return to the properties of the gluon in section 6.

E. Jet invariant mass - PLUTO

When jets were first discovered at SPEAR [36], the most useful quantity was the sphericity. At PETRA, a number of quantities have been found to be useful, including thrust, aplanarity, oblateness, and energy flow. These quantities all have the character of not being sensitive to missing particles and to the details of fragmentation. As the experiments

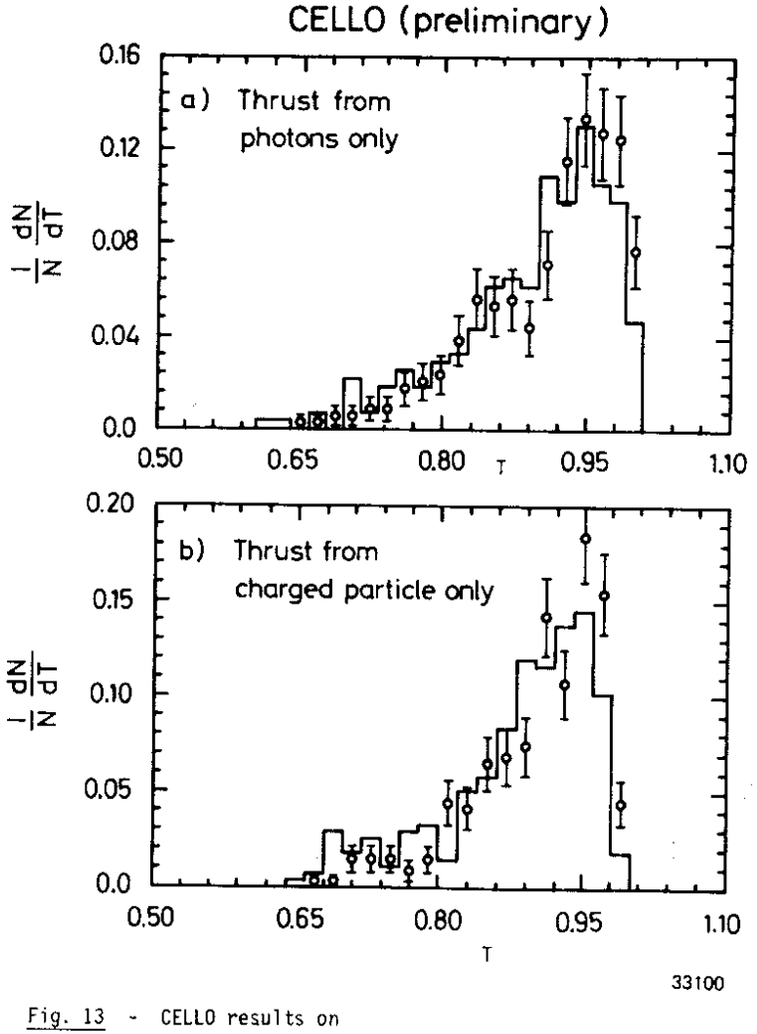

Fig. 13 - CELLO results on
a) thrust distribution reconstructed from photons only;
b) thrust distribution reconstructed from charged particles only.

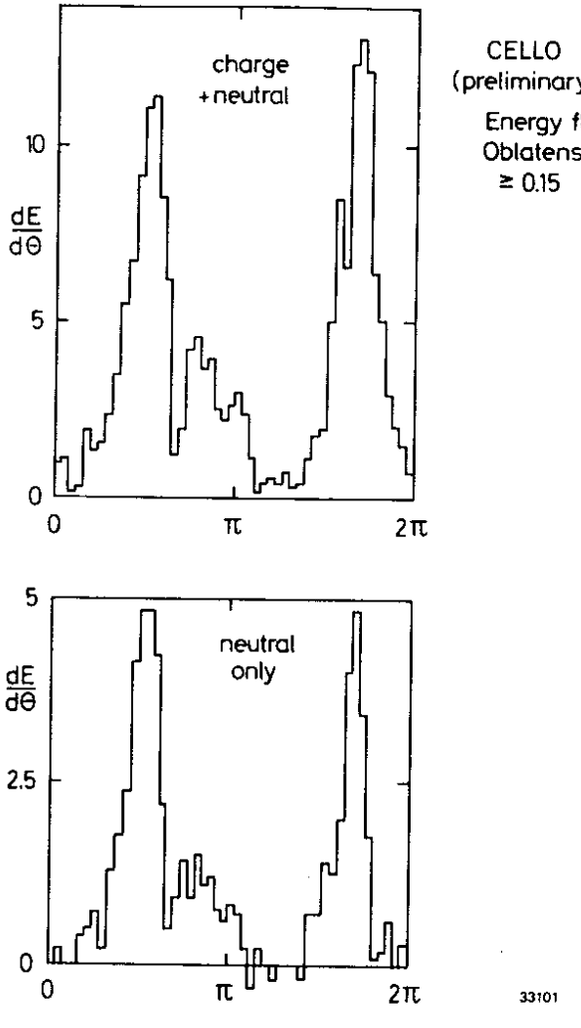

Fig. 14 - CELLO results on energy flow for the events with oblateness $\geq$ 0.15;
a) for charged and neutral particles
b) for neutral particles only.

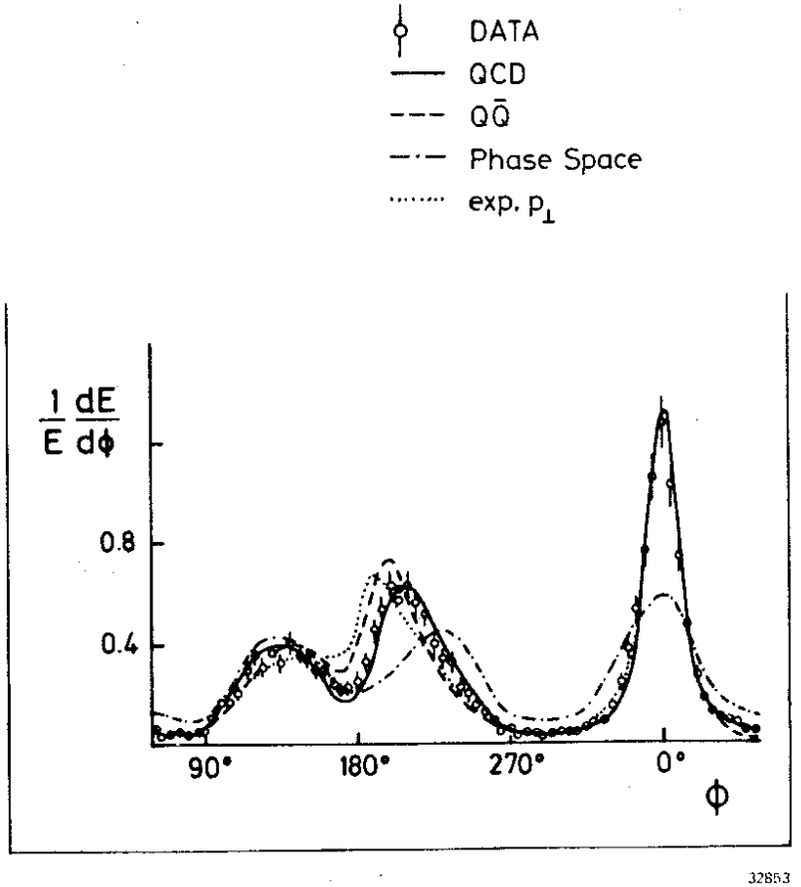

Fig. 15 -The energy flow distribution from MARK J Collaboration compared with the models of QCD, $q\bar{q}$, phase space, and a $q\bar{q}$ model with a $\exp(-P_T/650\ \text{MeV})$ fragmentation distribution.

continue to improve, the amount of missing particles decreases and the fragmentation process becomes better understood. Thus this advantage of the presently used quantities becomes less important, and it seems likely that other quantities may be profitably employed to gain a better understanding of the data.

A first step has been taken in this direction recently by PLUTO. They study the jet invariant mass proposed by Clavelli [37]. This is defined as follows for each event. Take all the measured particles, partition them into two sets, and calculate the invariant masses m_1 and m_2 of the two set by minimizing the sum of $(m_1^2 + m_2^2)$ over all partitions. PLUTO has carried out a Monte Carlo study, and it is found that the jet mass distribution for a generated sample of events is considerably degraded after imposing acceptance cuts and detector effects. Accordingly an eleborate correction procedure is necessary. Their result [38] is shown in Fig. 16 together with the QCD results of Hoyer et al. [11] with fragmentation, and leading log approximations [39] without fragmentation. It shows clearly sensitivity to fragmentation. As a first application of the jet invariant mass, it is shown [38] in Fig. 17 the dependence of charged multiplicity on the mass of the heavy jet (M_H) or of the light jet (M_L).

In the near future we expect to see more new and interesting variables used to analyze the experimental data of higher statistics.

6. PROPERTIES OF THE GLUON

A. Spin of the gluon - TASSO, PLUTO

Two years ago gluon bremsstrahlung was first observed at PETRA in the form of three-jet events [40-44]. The determination of the spin of the

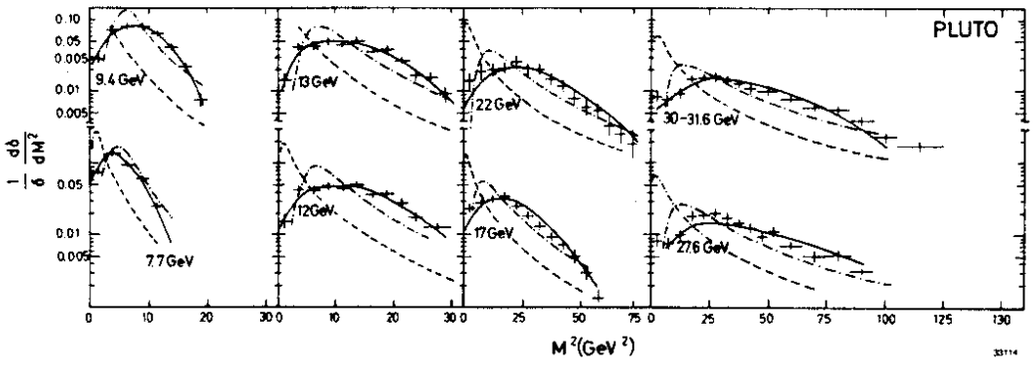

Fig. 16 - Normalized jet invariant mass distributions from 7.7 to 31.6 GeV. The solid curve represents the expectations from Hoyer et al. Monte Carlo. The dotted and dashed dotted curves show the predictions of a LL calculation ref. [39] for two different values of the QCD cut off parameter Λ of 200 MeV and 1.5 GeV respectively.

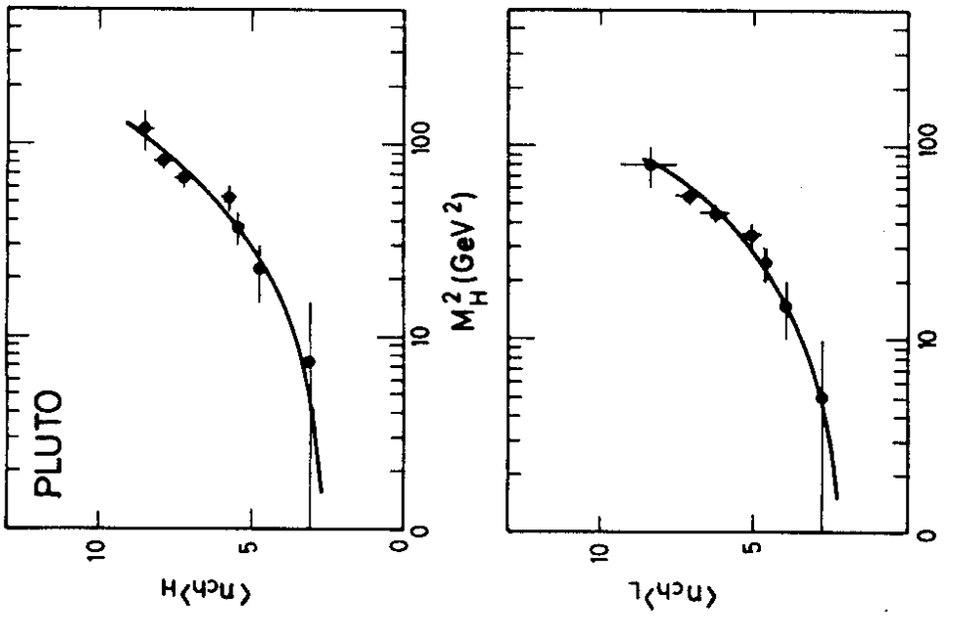

Fig. 17
The mean charged multiplicity of the heavy (M_H) and light (M_L) jets as a function of their masses M for the 27.6 - 31.6 GeV sample. The solid curves show the results of a fit to a QCD inspired form of

$$\langle n_{ch}\rangle = a + b \exp\left(c\sqrt{\ln M^2/\Lambda^2}\right) \qquad (M = M_L \text{ or } M_H)$$

with c = 2.4 and Λ = 500 MeV, a = 0.91 ± 0.19 (0.62 ± 0.19) and b = 0.019 ± 0.001 (0.021 ± 0.001) for the heavy (light) jets.

gluon is of obvious importance, but much more statistics was necessary to accomplish this.

For three-jet events define

$$x_j = E_j / E_B$$

where E_j is the energy of jet j and $E_B = \sqrt{s}/2$ is the incident beam energy. To the lowest order in the strong coupling constant α_s, the distribution in the Dalitz plot is then given by [45]:

$$\text{Vector}: \frac{1}{\sigma_0}\left(\frac{d\sigma}{dx_1 dx_2}\right)_V = \frac{2\alpha_s}{3\pi}\left[\frac{x_1^2 + x_2^2}{(1-x_1)(1-x_2)} + \text{permutations}\right]$$

$$\text{Scalar}: \frac{1}{\sigma_0}\left(\frac{d\sigma}{dx_1 dx_2}\right)_S = \frac{\tilde{\alpha}_s}{3\pi}\left[\frac{x_3^2}{(1-x_1)(1-x_2)} + \text{permutations}\right]$$

It is conventional to choose the x's such that $x_3 \leq x_2 \leq x_1$ and x_1 is the thrust. In order to discriminate between vector and scalar gluons, TASSO [46] uses the variable $\tilde{\theta}$ of Ellis and Karliner [47] which is the angle between the jet 1 and jet 2 in the center-of-mass system of jets 2 and jets 3 :

$$|\cos\tilde{\theta}| = \frac{x_2 - x_3}{x_1}$$

The result [46] is shown in Fig. 18, where the average values $\langle|\cos\tilde{\theta}|\rangle$ are shown in Table 5.

The conclusion is therefore reached that the spin of the gluon is indeed 1 and the result is insensitive to the details of jet fragmentation as shown in Table 5 and Fig. 18.

More recently PLUTO [48] uses instead the variable $x_\perp$ explained in the upper part of Fig. 19 :

$$x_\perp = \frac{2}{x_1}\left[(1-x_1)(1-x_2)(1-x_3)\right]^{1/2}$$

In terms of this $x_\perp$, the results are shown in Fig. 19. In this figure, PLUTO has used their previous determination of α_s for the case of the vector

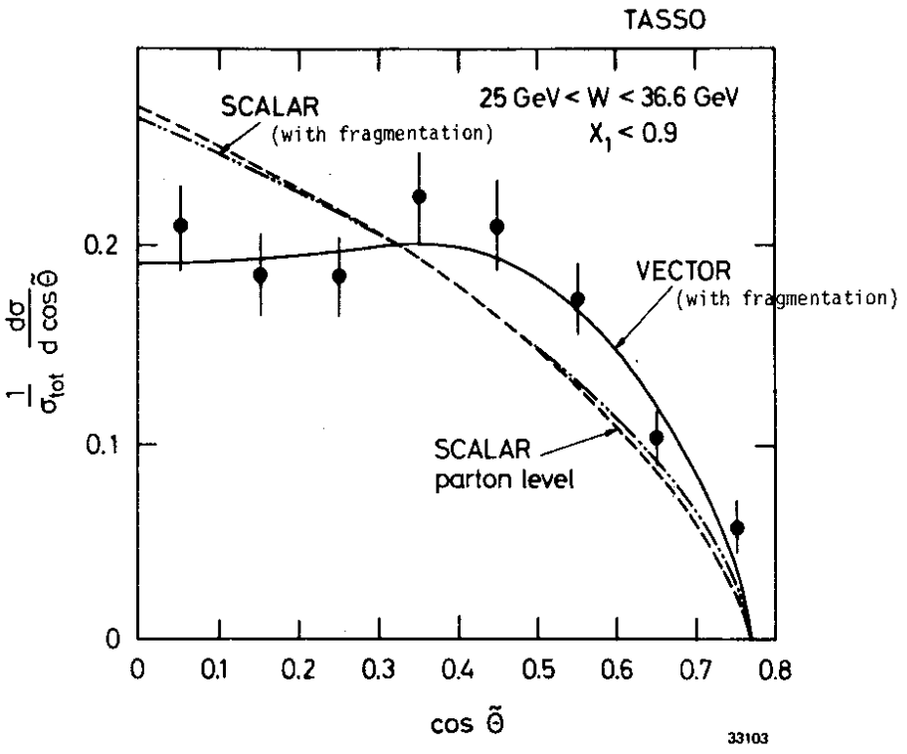

Fig. 18 - Observed distribution of the TASSO data in the region $x_1 < 0.9$ as a function of the cosine of the Ellis-Karliner angle $\tilde{\theta}$. The solid line shows the QCD Monte Carlo prediction , dashed line the prediction for the scalar gluons (— ·· — for Monte Carlo scalar model; — — — for scalar model of parton level). All curves are normalized to the number of observed events.

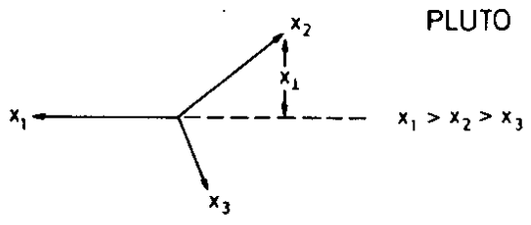

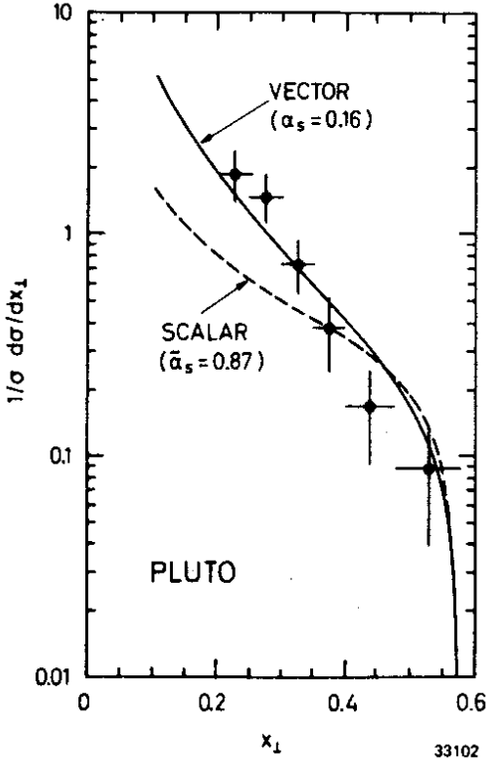

Fig. 19 - $x_\perp$ distribution from PLUTO compared with QCD (solid curve) and scalar gluon model (dashed curve).

gluon but the $\tilde{\alpha}_s$ for the scalar gluon is fitted. Thus the χ^2 is 5.7 for six degrees of freedom in the vector case, and 19.7 for five degrees of freedom in the scalar case. Again the spin of the gluon is determined to be 1.

Alternative methods of analysis have also been applied to these data from PLUTO [49] and TASSO [50] leading to the same value of the gluon spin.

Table 5 - Average value for $|\cos\tilde{\theta}|$

	$\langle\|\cos\tilde{\theta}\|\rangle$	Standard deviation
Data	0.339 ± 0.008	
Vector (Monte Carlo) with acceptance and jet fragmentation	0.341 ± 0.003	$0.2\ \sigma$
Vector (parton level prediction) no acceptance cut no jet fragmentation	0.348	$1.1\ \sigma$
Scalar (Monte Carlo)	0.298 ± 0.003	$4.8\ \sigma$
Scalar (parton level prediction)	0.298	$5.1\ \sigma$

B. Differences between quark and gluon jets - JADE

Ever since the first observation of gluon jets, an intriguing question is: how do we distinguish a gluon jet from a quark jet ? Although some differences are expected from QCD, these two kinds of jets turn out to be remarkably similar. For example, JADE has measured the ratio of photon energy to charged particle energy separately for the three jets, and the results are [30] :

Jet 1 : 0.47 ± 0.01 ;

Jet 2 : 0.46 ± 0.01 ;

Jet 3 : 0.44 ± 0.02 ;

where the errors are statistical but the systematic errors are expected to be small.

The first attempt to distinguish these two kinds of jets has very recently been reported by JADE [51]. At the same jet energy, the average transverse momentum $\langle p_\perp \rangle$ of particles with respect to the jet axis is larger for the gluon jet than for the quark jet. This result is very preliminary, and has not been confirmed by other groups at PETRA. It still needs a great deal of more study.

JADE starts with 4955 hadronic events in the energy range of $\sqrt{s}$ between 30 to 36 GeV. Planar three-jet events are selected as described in Reference [52] with the cut $Q_2 - Q_1 \geq 0.07$ and $Q_1 \leq 0.06$ where Q_1, Q_2 and Q_3 are the normalized eigenvalues of the sphericity tensor with $0 \leq Q_1 \leq Q_2 \leq Q_3 \leq 1$. To identify 3 jets of particles in a planar event and to determine the jet direction vectors, the three-jet analysis method of Reference [53] was used with the modification of maximizing thrust instead of minimizing sphericity. Events in which one or more of the jets contain fewer than 4 particles or an energy of less than 2 GeV are rejected. 596 events meet these criteria. The three jets are ordered according to the angles between their direction vectors, projected into the event plane.

By Monte Carlo calculation using the LUND model it is found, with the ordering of reconstructed energies: $E_{jet1} > E_{jet2} > E_{jet3}$, that in 51% of the events jet 3 is the gluon jet; 22% jet 2 is the gluon jet; 12% jet 1 is the gluon jet; and 15% the event is actually a two-jet event without a gluon jet.

The observed [52] $\langle p_\perp \rangle$ is shown in Fig. 20 for the three jets separately as function of the visible jet energy. It is seen that, for the same visible jet energy, $\langle p_\perp \rangle$ is larger for jet 3 than for jet 1 and 2.

The difference is not present in the Monte Carlo of Hoyer et al.[11], where the fragmentations of gluon and quark jets are identical. It is seen in the LUND Monte Carlo [8,13] where the gluon is associated with a kink in the color force field. Thus the experimental result of JADE agrees with LUND but not with Hoyer et al.

The question has been raised whether the effect is due to the use of the visible jet energy as the variable. Thus a further cut is introduced :

$$|E_{jet} - E_{jet}^{visible}| \leq 0.2\, E_{jet},$$

where E_{jet} is the jet energy calculated from the directions of the three jet axes. The result is shown in Fig. 21.

A great deal more effort is expected to be spent at PETRA on finding differences between gluon and quark jets. It is hoped that this knowledge will deepen our understanding of the physics of electron-positron annihilation.

7. TWO-PHOTON PHYSICS

A. $\gamma\gamma \to \rho^o\rho^o$ - TASSO, CELLO

A year ago, the TASSO Collaboration observed the $\gamma\gamma \to \rho^o\rho^o$ process [54] which exhibits a large enhancement near the threshold.

Since each ρ^o decays into a $\pi^+\pi^-$ pair, experimentally

$$e^+e^- \to e^+e^- \pi^+\pi^+\pi^-\pi^-$$

is observed. It is therefore possible to use the untagged events, and furthermore no extrapolation to $Q^2 = 0$ is needed. The events are identified by two positive and two negative tracks such that

$$\left|\sum_{j=1}^{4} \vec{p}_{jT}\right| < 0.15 \text{ GeV/c},$$

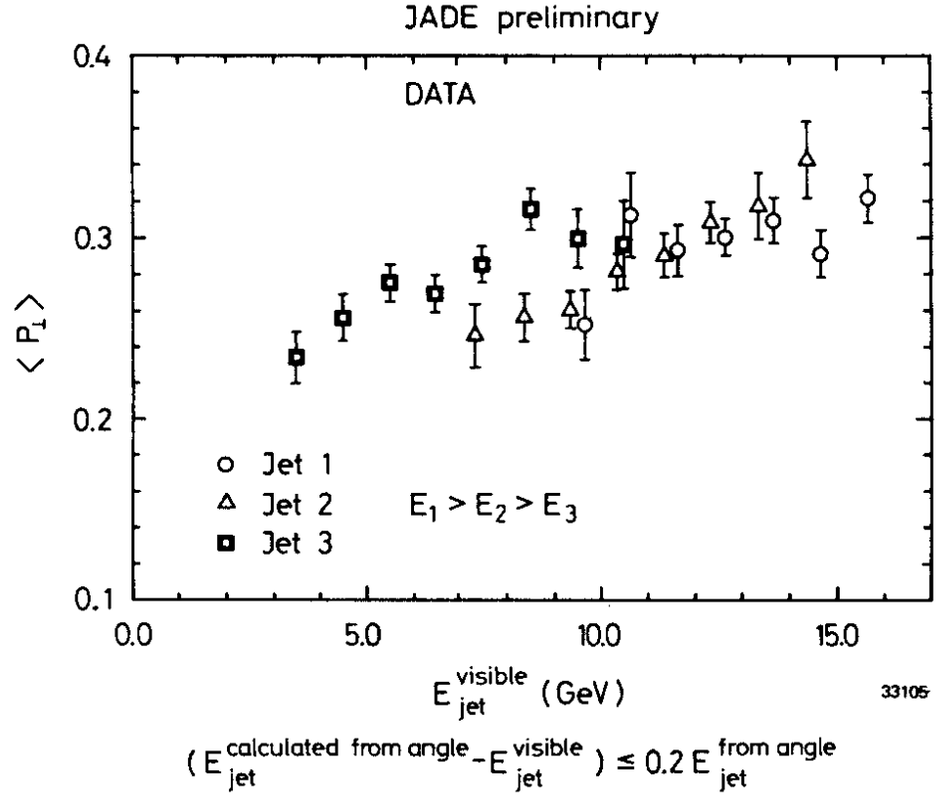

$$(E_{jet}^{calculated\ from\ angle} - E_{jet}^{visible}) \leq 0.2\, E_{jet}^{from\ angle}$$

Fig. 21

Average $P_\perp$ distribution from JADE for the highest energy jets (E_1) medium energy jets (E_2) and lowest energy jets (E_3) as a function of visible energies of the jets. Visible energies of the jets are required to be within 20% of the calculated energies of the jets.

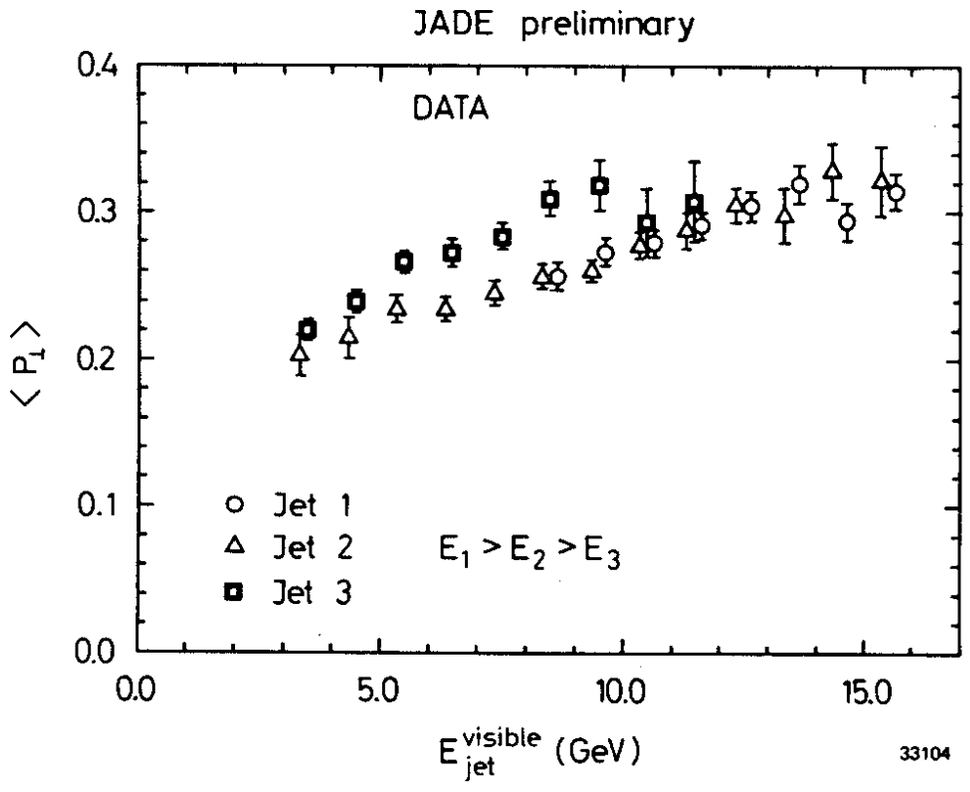

Fig. 20

Average $P_\perp$ distribution from JADE for the highest energy jets (E_1) medium energy jets (E_2) and lowest energy jets (E_3) as a function of visible energies of the jets.

where p_{jT} is the transverse momentum with respect to the beam axis. In the range $1.5 < W < 2.3$ GeV, 89 events are found that satisfy this cut. The TASSO result is shown in Fig. 22, where it is seen that for $W < 2$ GeV, the cross section for $\gamma\gamma \to \rho^0\rho^0$ peaks strongly near threshold and drops rapidly with energy and is very much larger than that expected from the vector-meson dominance model.

Recently, the published results of MARK II [55] at SPEAR and the preliminary result of CELLO [56] at PETRA show a large cross section for $\gamma\gamma \to \pi^+\pi^-\pi^+\pi^-$ with 4π invariant mass extended below that of TASSO. The results of the $\gamma\gamma \to \pi^+\pi^-\pi^-\pi^-$ from MARK II and CELLO (preliminary) are shown in Fig. 23 together with the TASSO cross section for $\gamma\gamma \to \rho^0\rho^0$. This MARK II 4π cross section is consistent with the two-photon signal being all $\gamma\gamma \to \rho^0\rho^0$, but cannot rule out a $\gamma\gamma \to 4\pi$ (phase space) component as large as 15 to 20% in a given mass bin. The results of large cross section at low 4π invariant mass from MARK II and CELLO rule out the prediction of two theoretical models which tried to fit the TASSO published result alone as shown in Fig. 23. Layssac and Renard [57] tried to explain the TASSO results with a superposition of the f and ε mesons together with a large contribution from a hypothetical resonance G at 1.6 GeV, whereas Goldberg and Weiler [58] fitted it with a superposition of the $f^0(1270)$ and a $J^{PC} = 2^{-+}$, $I = 0$ resonance with mass ≈ 1.66 GeV and width ≈ 0.2 GeV.

C. $\gamma\gamma \to$ large P_T jets - TASSO, JADE, PLUTO

In the old idea of vector meson dominance, $\gamma\gamma$ processes were considered to be similar to, for example, pp or πp processes. On the other hand, in the quark picture, the diagram of Fig. 24 [59] is important for large momentum transfer, although there is no analog in pp or πp scattering. It is therefore important to study consequences of this diagram through events of the type

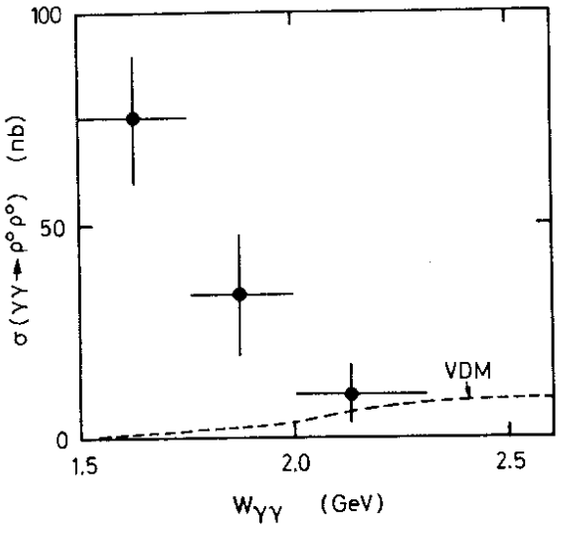

Fig. 22 - Cross section for $e^+e^- \to e^+e^- \rho^0\rho^0$ as measured by TASSO. An asymptotic VMD prediction is shown as the dotted line.

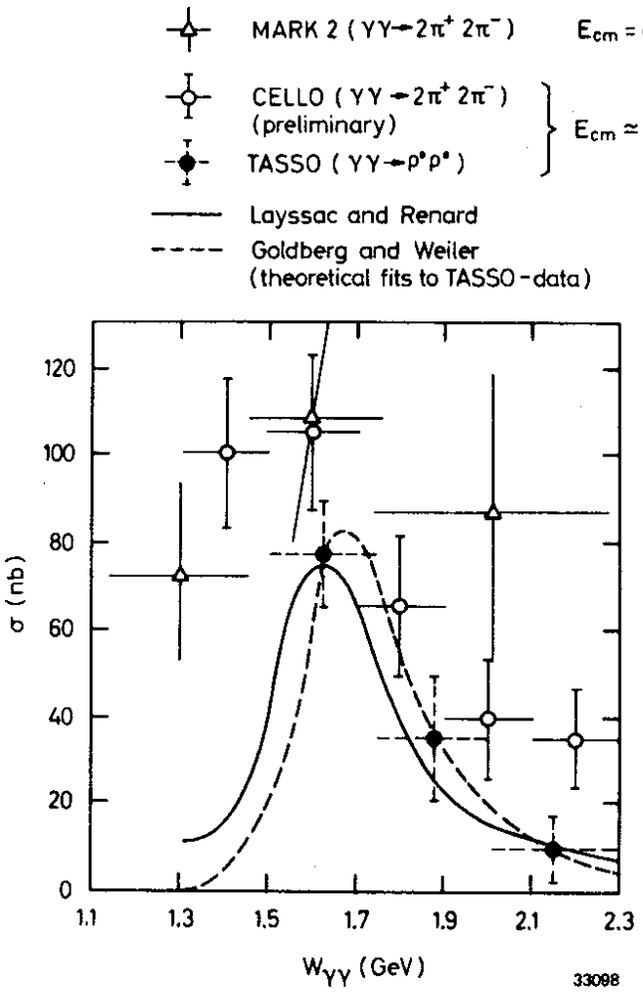

Fig. 23 - Cross sections of the processes $\gamma\gamma \to \pi^+\pi^-\pi^+\pi^-$ (MARK J and CELLO) and $\gamma\gamma \to \rho^0\rho^0$ (TASSO) in comparison with two theoretical models.

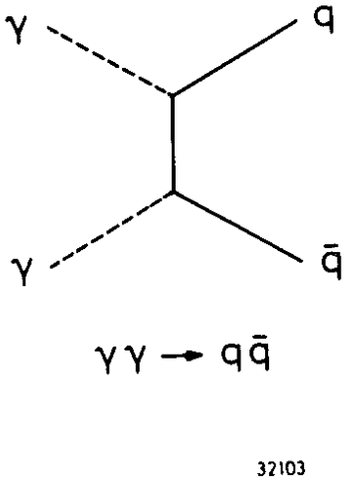

Fig. 24 - Diagram for the creation of a $q\bar{q}$ pair in $\gamma\gamma$.

$$e^+e^- \rightarrow e^+e^- + \text{two jets},$$

where the jets are not collinear but are coplanar with the beam direction. A single-tagged event of this type from TASSO is shown in Fig. 25.

The main characteristic of the hard scattering diagram of Fig. 24 is the ratio [60]

$$R = \frac{\sigma(\gamma\gamma \rightarrow q\bar{q})}{\sigma(\gamma\gamma \rightarrow \mu^+\mu^-)} = 3\Sigma_{u,d,s,c} Q_i^4, \quad Q_i^4 = \frac{34}{27} \qquad (Q_i = \text{quark charge})$$

if the first four quark flavors are included. Note that u and c are responsible for 94% of this $R_{\gamma\gamma}$. Similar to $\gamma\gamma \rightarrow \mu^+\mu^-$, the differential cross section $d\sigma/dp_T^2$ falls roughly as $\bar{p}_T^4$, where p_T is the transverse momentum of each hadronic jet with respect to the beam direction. This is a much slower decrease than that exhibited by pp and πp cross sections. The TASSO single-tag data [61] is shown in Fig. 26 and compared with the vector dominance model (dotted line) and $\gamma\gamma \rightarrow q\bar{q}$ (shadded area), both with acceptance effects taken into account. At large p_T, the data approach the prediction for the $\gamma\gamma \rightarrow q\bar{q}$ process, while VDM contribution would be much too small to explain the observed differential cross section. Similar results have also been obtained by JADE [62] and PLUTO [63] and those from JADE are shown in Fig. 27. It is interesting to note from both Fig. 26 and Fig. 27 that even at the highest p_T^2 the experimental data tend to be somewhat higher, by a factor of about 1.5 than the expectation evaluation from the diagram of Fig. 24. The reason may be the contributions from QCD corrections, from 3- and 4-jet processes, and from higher twist diagrams [64] which have not yet been incorporated in the calculation.

D. Deep inelastic eγ scattering - PLUTO

Recently, PLUTO [65] obtained interesting first results on the structure function of the photon. This is accomplished by using the large angle tagging. Since the other electron or positron is not tagged, the

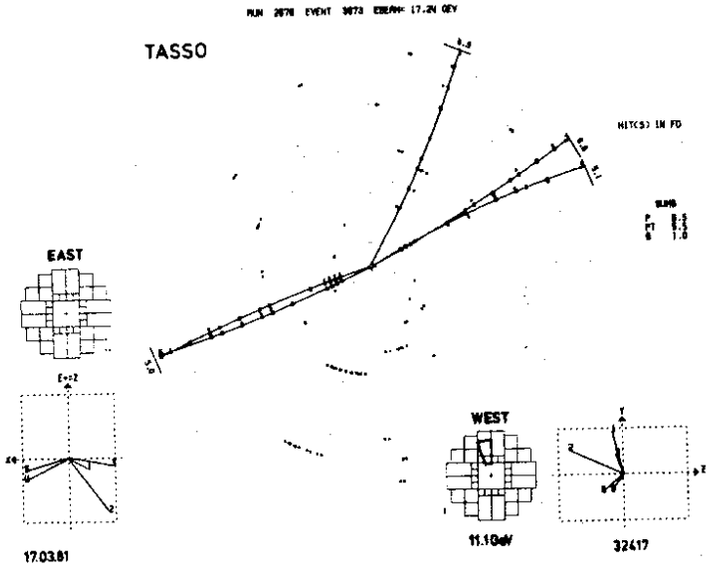

Fig. 25 - $\gamma\gamma \rightarrow$ 2 jet event of TASSO at $E_{c.m.} = 34.5$ GeV. The energy of the single tagged e^- is 11 GeV.

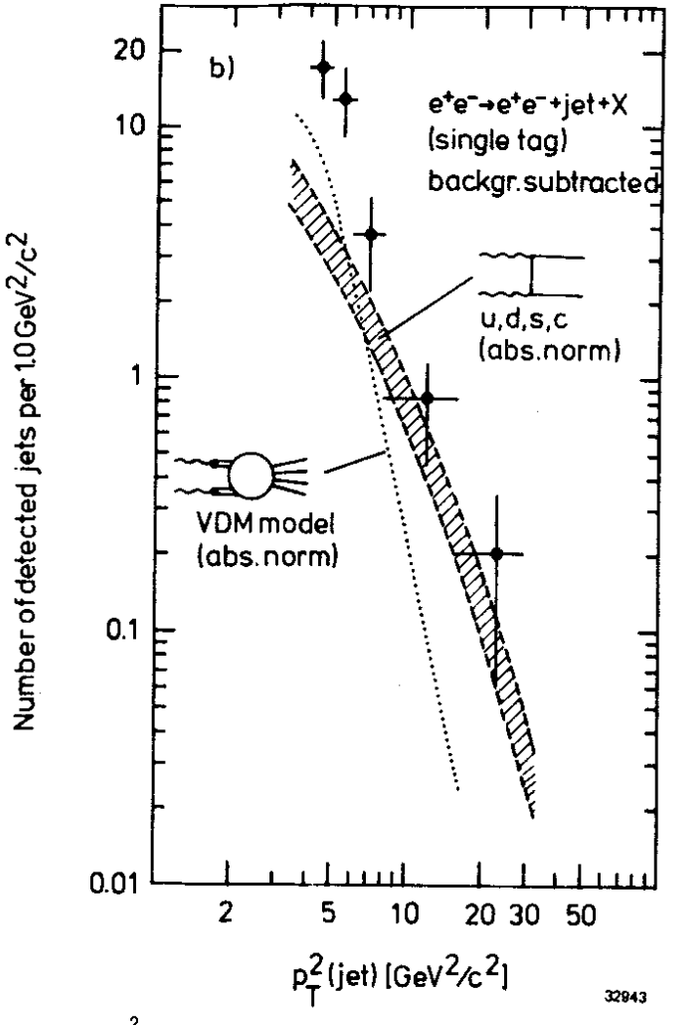

Fig. 26 - The P_T^2(jet) distribution from single tagged data of TASSO for $e^+e^- \to e^+e^-$ + jet + X, compared to a $e^+e^- \to e^+e^-$ + $q\bar{q}$ calculation with four different types of fragmentation model (shadded band) and to VDM (dotted line).

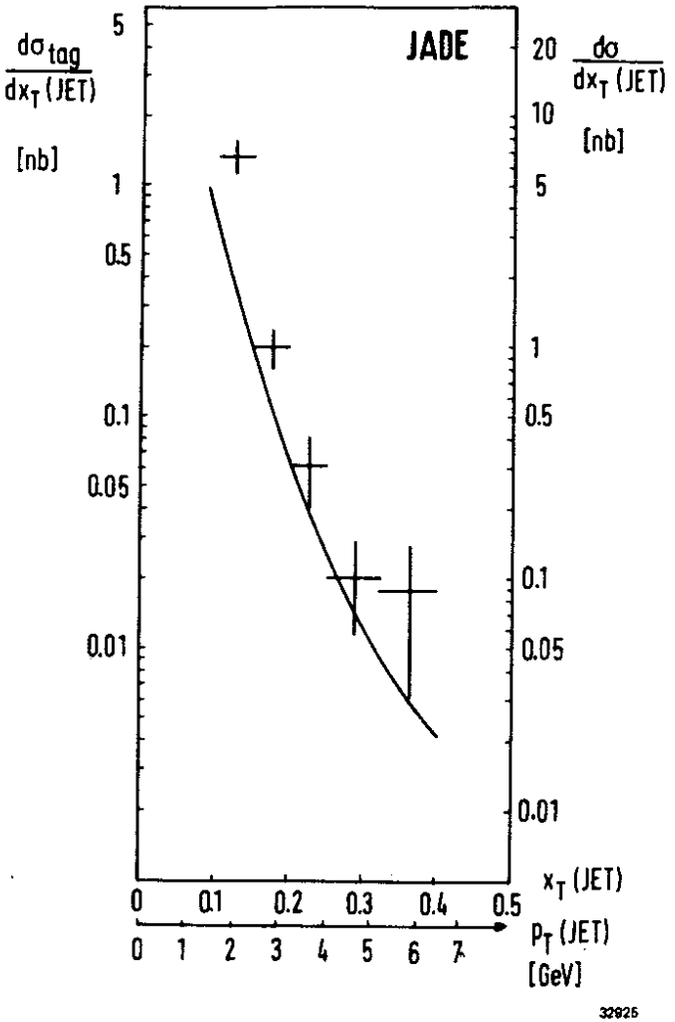

Fig. 27 - Transverse momentum distribution of jets for single tag data of JADE compared with absolute predictions for fractional charged quarks (curve). $x_T(JET) = p_T(JET)/E_{beam}$ is taken with respect to the centre of mass direction of motion. The cross section is given for the JADE tagging condition on the lefthand scale and integrated over all electron angles and energies on the righthand scale.

second photon is nearly on mass shell. Accordingly under this configuration the observed $e^+e^- \to e^+e^-$ + hadrons is closely related to the deep inelastic $e\gamma$ scattering as shown in Fig. 28(a), analogous to, for example, deep inelastic νp scattering.

There are several contributions to this diagram of Fig. 28(a). Vector dominance model gives the diagram of Fig. 28(b), while the QCD process $\gamma\gamma \to q\bar{q}$ of Fig. 24 leads to Fig. 28(c), and higher QCD corrections give diagrams such as that of Fig. 28(d).

The usual scaling variables x and y are defined as (see Fig. 29)

$$x = \frac{|Q_1^2|}{|Q_1|^2 + W^2} \quad \text{and} \quad y = 1 - \frac{E_1}{E}\cos^2\frac{\theta_1}{2}$$

With the experimental acceptance of PLUTO, xy^2 is small. Thus the cross section is well approximated by

$$\frac{d\sigma}{dxdy}\Big|_{e\gamma\to ex} = \frac{16\pi\,\alpha^2\,EE_\gamma}{Q^4}(1-y)\,F_2\,(x,\,Q^2)$$

where $Q^2 = |Q_1^2|$ and E_γ is the laboratory system energy of the nearly on-shell 'target' photon. In the quark model x is the relative momentum fraction of the quark and F_2 is a measure of the momentum weighted quark content of the photon target $F_2 \sim \Sigma\, e_i^2\, x \cdot q(x,Q^2)$.

On the basis of 111 background subtracted events, the result of PLUTO is shown in Fig. 30 and compared with a number of theoretical calculations [66-72]. It is clearly seen that the vector dominance diagram of Fig. 28(b) contributes only a small part of F_2, while the agreement with QCD is quite good.

QCD also predicts a Q^2 dependence of F_2 at fixed x, equivalent to a strong scale breaking. PLUTO has investigated this effect by plotting in Fig. 31 F_2 versus Q^2, averaged over $0.2 < x_{vis} < 0.8$. This restriction

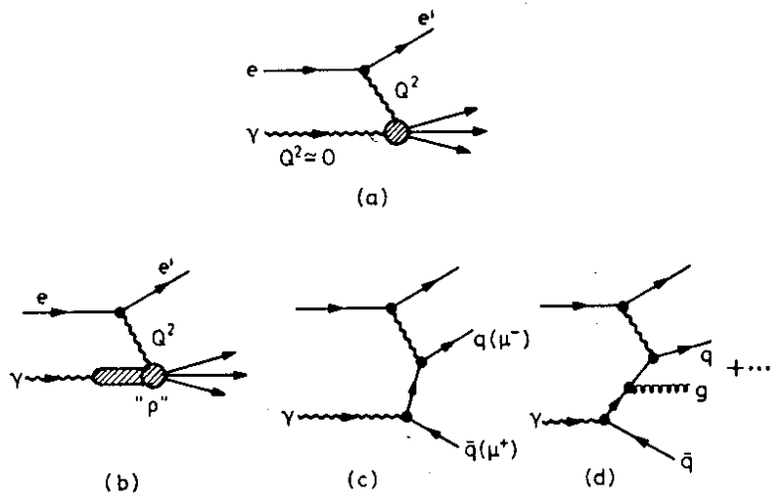

Fig. 28 - Diagrams contributing to e γ → e' hadrons.

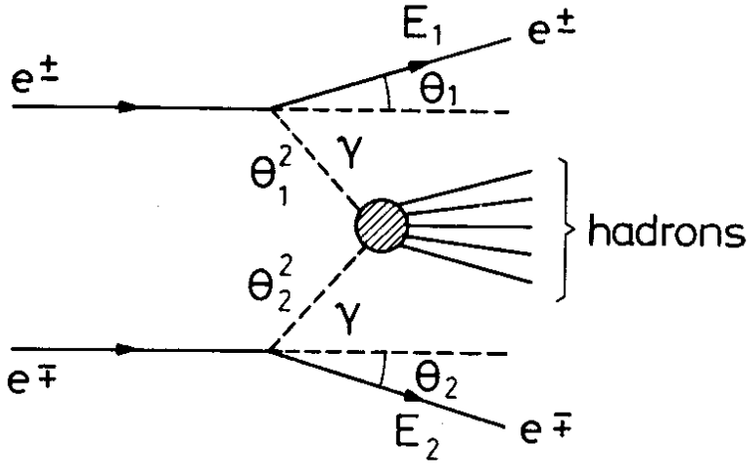

15.12.80

32104

Fig. 29 - Diagram for e^+e^- → e^+e^- + hadrons.

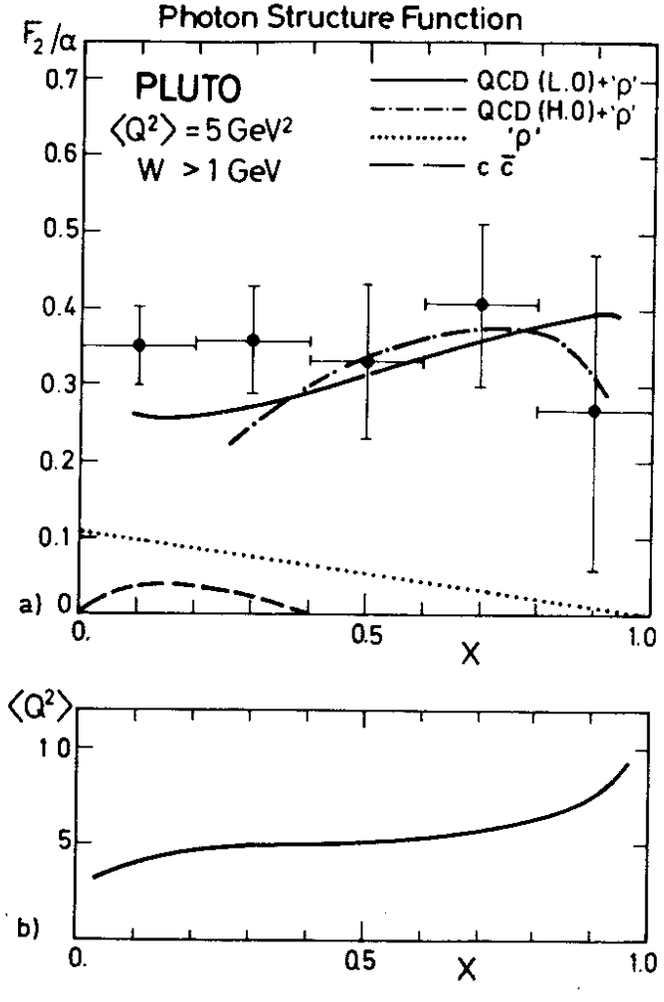

32962

Fig. 30 - Photon structure function $F_2(x)/\alpha$.
The data are averaged over $1 < Q^2 < 15$ GeV^2.

. . . . Hadronic structure function $F_{2,\rho}$ from diagram 28(b)

——— $F_{2,QCD} + F_{2,\rho}$ (Λ = 0.3 GeV, u,d,s quarks from diagrams 28(b), (c) and (d) to the leading order)

—.— $F_{2,QCD} + F_{2,\rho}$ (Λ = 0.3 GeV, u,d,s quards from diagrams 28(b), (c) and (d) including higher order correction)

- - - $F_{2,box}$ for c quarks only (m_q = 1.5 GeV from diagram 28(c)).

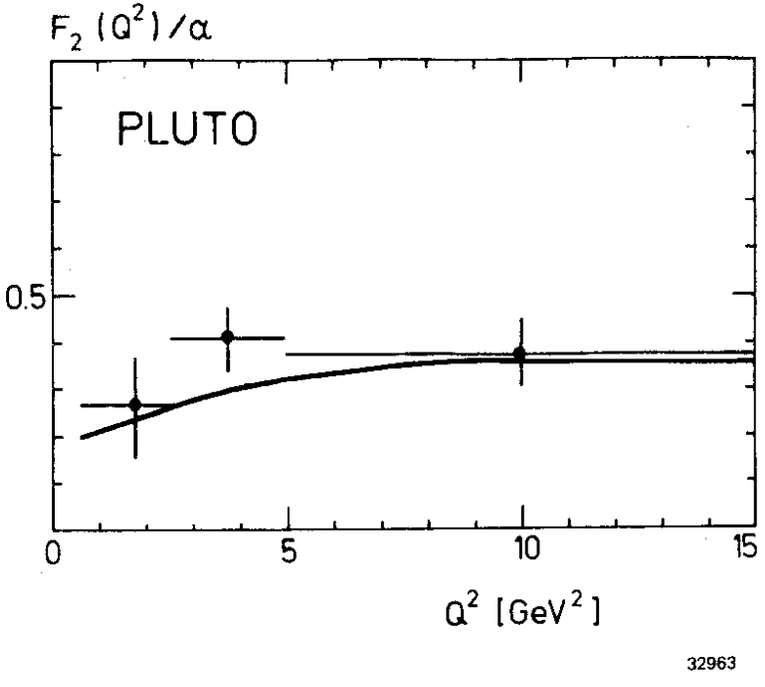

Fig. 31 - Photon structure function $F_2(q^2)/\alpha$.
The data are averaged over $0.2 < x_{vis} < 0.8$.
The curve shows the QCD prediction in the leading logarithm approximation with
$\Lambda = 0.3$ GeV.

on x is necessary in order to avoid Q^2-x correlations (see Fig.30(b)), which could also simulate a scale breaking. The data are clearly consistent with the QCD prediction in the leading order (solid line).

8. ELECTROWEAK INTERACTION

We now come to perhaps the most exciting recent result from PETRA, the observation of weak and electromagnetic interference. Indeed, it was one of the main original purposes of building PETRA to observe such effect.

A. Standard Model

The Standard Model is the elegant model of unified weak and electromagnetic interaction developed by Glashow [73], Weinberg [74], and Salam [75]. In this model, the process

$$e^-e^+ \to f\bar{f}$$

can proceed not only through one-photon annihilation (Fig. 32a) but also through one-Z^0 annihilation (Fig. 32b), where f can be any fundamental fermion: e^-, μ^-, τ^-, ν_e, ν_μ, ν_τ, u, d, s, c, b or the yet unobserved top quark t. Neglecting radiative corrections, the differential cross section for this process is, in the standard model with the quark mass neglected,

$$\frac{d\sigma(e^-e^+ \to f\bar{f})}{d\cos\theta} = \frac{\pi\alpha^2}{2s}\{Q_f^2(1+\cos^2\theta) - \frac{2Q_f\, g\, s\,(s/M_z^2-1)[v_e v_f(1+\cos^2\theta)+2a_e a_f\cos\theta]}{(s/M_z^2-1)^2+\Gamma_z^2/M_z^2} + \frac{s^2g^2[(v_e^2+a_e^2)(v_f^2+a_f^2)(1+\cos^2\theta)+8v_e a_e v_f a_f\cos\theta]}{(s/M_z^2-1)^2+\Gamma_z^2/M_z^2}\} \quad (8.1)$$

where M_z and Γ_z are the mass and width of Z^0, and

$$g = \frac{\sqrt{2}\,G_F}{4e^2} = \frac{\sqrt{2}\,G_F}{16\pi\alpha} \quad (8.2)$$

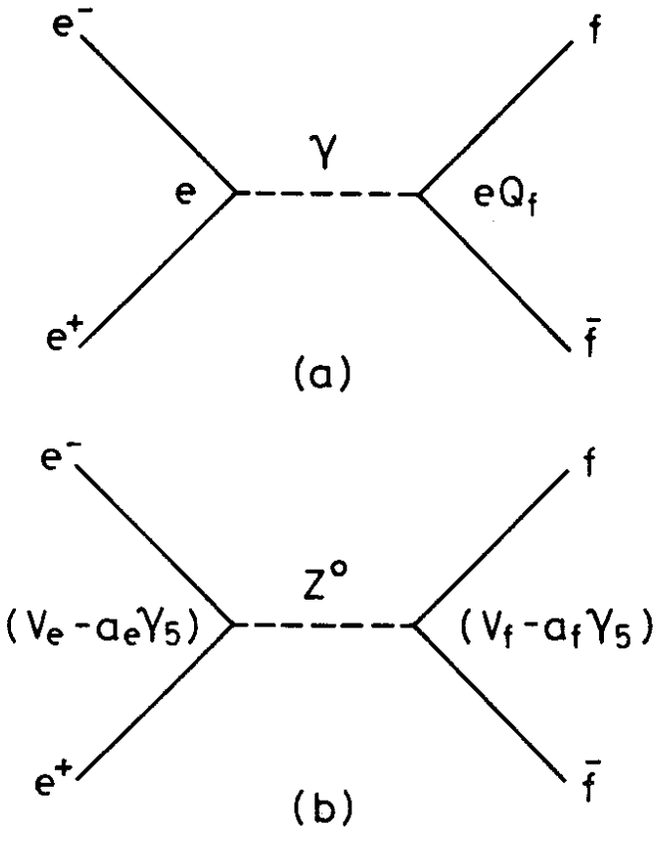

Fig. 32 - The process $e^-e^+ \to f\bar{f}$ in the Standard Model.

in terms of the Fermi weak coupling constant G_F. The values of v and a in the Standard Model for various fermions are tabulated in Table 6. Integration over θ gives in particular

$$R_f = Q_f^2 - \frac{2Q_f\, g\, s\, (s/M_z^2 - 1)\, v_e\, v_f - s^2g^2\, (v_e^2 + a_e^2)(v_f^2 + a_f^2)}{(s/M_z^2 - 1)^2 + \Gamma_z^2/M_z^2} \qquad (8.3)$$

In both of these formulas, the color factor 3 has not been included when the fermion is a quark.

Table 6 - Values of v_f and a_f in the Standard Model

f	e^-, μ^-, τ^-	d, s, b	u, c, t
Q_f	- 1	$-\frac{1}{3}$	$\frac{2}{3}$
v_f	$-1+4\sin^2\theta_W$	$-1+\frac{4}{3}\sin^2\theta_W$	$1-\frac{8}{3}\sin^2\theta_W$
a_f	- 1	- 1	1

At PETRA energies, Γ_z is of no consequence. Also, the total cross section is more sensitive to v than to a, while the forward-backward asymmetry is more sensitive to a than to v. This asymmetry has the angular dependence

$$\frac{\cos\theta}{1+\cos^2\theta},$$

which is largest for $\theta = 0, \pi$. This has the consequence that the experimental observed asymmetry depends significantly on the acceptance of the detector.

B. Determination of $\sin^2\theta_W$ - MARK J, JADE

At the highest PETRA energy of 37 GeV, the dimensionless quantity gs, with g defined by (8.2) is about 0.06. Since this is quite sizable, ac-

curate measurements of the various cross sections can be used to determine the Weinberg angle [74] θ_W. This analysis has been carried out by MARK J [76] and JADE [77]. Of course, QCD and QED corrections need to be taken into account. It should be remembered that, in the Standard Model, the mass M_z also depends on θ_W.

The resulting values of $\sin^2\theta_W$ from JADE and MARK J are

	JADE	MARK J
From hadron events only ($e^-e^+ \to q\bar{q}$)	0.22 ± 0.10 or 0.56 ± 0.10	$0.27\ ^{+\ 0.34}_{-\ 0.08}$
From hadron and lepton events ($e^-e^+ \to q\bar{q}$, $\mu^-\mu^+$, $\tau^-\tau^+$, e^+e^-)	0.22 ± 0.08	0.27 ± 0.08

These results provide the first indication that (i) weak neutral current couples to all known quarks, since over 40% of the hadronic events involve a heavy quark, either c or b; (ii) the Standard Model is valid in the time-like region up to 1350 GeV^2.

C. Forward-backward asymmetry

Because of parity non-conservation in weak interactions, a dramatic effect of the interference between the one-photon annihilation of Fig. 32(a) and the one-Z^0 annihilation if Fig. 32(b) is the forward-backward asymmetry in $e^-e^+ \to f\bar{f}$. This is clearly seen as the $\cos\theta$ terms in eq.(8.1). Very recently, this asymmetry was observed for the first time in the process

$$e^-e^+ \to \mu^-\mu^+ .$$

This gives one of the direct and beautiful experimental verifications of the Standard Model. We give here a detailed description of how this result is obtained.

In Table 7, the observed asymmetries $A_{\mu\mu}$ and $A_{\tau\tau}$ by JADE, MARK J, PLUTO, and TASSO with radiative corrections removed are given for both $e^-e^+ \to \mu^-\mu^+$ and $e^-e^+ \to \tau^-\tau^+$, together with the expected theoretical values from the Standard Model. The differences between the expected theoretical values for the various collaborations are due to the variation of the acceptances of the detectors, as already discussed at the end of section A. Only the value for $A_{\mu\mu}$ from TASSO has been corrected for acceptance. These data were obtained with an average s of

$$\langle s \rangle \ \sim \ 1100 \text{ GeV}^2.$$

Clearly the data on the τ asymmetry is as yet not significant.

Table 7 - Forward-backward asymmetry of $e^-e^+ \to \mu^-\mu^+$ and $e^-e^+ \to \tau^-\tau^+$

	JADE	MARK J	PLUTO	TASSO	combined
$A_{\mu\mu}$(%)	-11 ± 4	-3 ± 4	7 ± 10	-11.3 ± 5.0	-7.7 ± 2.4
expected	-7.8	-7.1	-5.8	-8.7	-7.8
$A_{\tau\tau}$(%)		-6 ± 12		0 ± 11	-2 ± 8
expected		-5		-7	-6

Branson [78] has combined these four sets of data on the μ asymmetry to get the value, as given in Table 7, of

$$(-7.7 \pm 2.4)\%$$

compared with the theoretical expected value of -7.8%. PETRA has therefore observed a forward-backward asymmetry in $e^-e^- \to \mu^-\mu^+$ which is in good agreement with the Standard Model, and is 3.2 standard deviations away from 0. If the preliminary CELLO data of $(-1.3\ ^{+\ 8}_{-10})\%$ is also included, the result changes by less than a tenth of a standard deviation.

In general, combining data from different experiments may be considered problematic. However, in the present case, the situation is favorable for at least two reasons: first all the experiments have been carried out simultaneously on the same accelerator PETRA, and, secondly, there is no known systematic error comparable to the present statistical error in the measurement of the forward-backward asymmetry. Therefore it is perfectly reasonable to think of this asymmetry measurement as one big experiment at PETRA.

There only remains a technical problem of taking into account the different acceptances as reflected in the theoretical expected values. Branson [78] solved this problem by considering only the ratio of the observed and theoretical asymmetries. Let

$$\gamma = \frac{A_{\mu\mu}\,|_{\text{observed}}}{A_{\mu\mu}\,|_{\text{expected}}}$$

then these ratios are

JADE	1.14 ± 0.51
MARK J	0.42 ± 0.56
PLUTO	-1.21 ± 1.72
TASSO	1.30 ± 0.57

These four values are then averaged using as weights the errors to the -2 power:

$$\frac{1.41(0.51)^{-2} + 0.42(0.56)^{-2} - 1.21(1.72)^{-2} + 1.30(0.57)^{-2}}{(0.51)^{-2} + (0.56)^{-2} + (1.72)^{-2} + (0.57)^{-2}} = 0.99.$$

From the point of view of one big experiment, the errors combine in the usual way to give an combined γ of

$$\gamma = 0.99 \pm 0.31$$

It is not crucial what value is used for the combined theoretical expected value. With -7.8%, the combined experimental value of $(-7.7 \pm 2.4)\%$ is obtained.

Acknowledgements

I wish to thank Professors G.Feldman, F.Gilman and D.W.G.S.Leith for their hospitality at The 1981 SLAC Summer Institute on Particle Physics. I am grateful to Professors R.Kose, T.Meyer, G.Rudolph, K. Steffen, P.Söding, B.H.Wiik, G.Wolf, and G.Zobernig for helpful and stimulating discussions. Finally I would like to thank the University of Wisconsin and DESY for their support.

REFERENCES

1) K.Robinson and G.A.Voss, CEA Report CEA-TM-149 (1965)

2) K.Steffen, Internal Report DESY M-79/07 (1979)

3) K.Steffen, G.A.Voss, and G.Wolf, Internal Report DESY M-81/20 (1981)

4) TASSO Collaboration, R.Brandelik et al., Phys.Lett.94B, 444 (1980)

5) JADE Collaboration, W.Bartel et al., Phys.Lett. 104B, 325 (1981)

6) TASSO Collaboration, R.Brandelik et al., Phys.Lett. 105B, 75 (1981)

7) B.Andersson, G.Gustafson, and T.Sjoestrand, Lund preprint LU TP 81-3 (1981)

8) J.Andersson, G.Gustafson, and C.Peterson, Nucl.Phys.B135, 273 (1978)

9) R.D.Field and R.P.Feynman, Nucl.Phys.B136, 1 (1978)

10) T.Meyer of TASSO Collaboration, private communication

11) P.Hoyer, P.Osland, H.G.Sander, and T.F.Walsh, Nucl.Phys. B 161, 349 (1979)

12) A.Ali, E.Pietarinen, G.Kramer, and J.Willrodt, Phys.Lett. 93 B, 155 (1980)

13) J.B.Andersson, G.Gustafson, and T.Sjoestrand, Phys.Lett. 94B, 211 (1980)

14) M.Piccolo et al., Phys.Rev.Lett. 39, 1503 (1977)

15) G.S.Abrams et al., Phys.Rev.Lett. 44, 10 (1980)

16) T.Meyer, DESY Report 81/046 (1981)

17) D.Cords, rapporteur talk, Proceedings of the XXth International Conference on High Energy Physics, Madison, Wisconsin, USA, July 17-23, 1980

18) PLUTO Collaboration, J.Burmeister et al., Phys.Lett. 67B 367 (1977)

19) SLAC-LBL Collaboration, V.Lüth et al., Phys.Lett.70B, 120 (1977)

20) PLUTO Collaboration, Ch.Berger et al., DESY Report 81/018 (1981)

21) TASSO Collaboration, R.Brandelik et al., Phys.Lett.94B, 91 (1980)

22) DELCO Collaboration, W.Bacino et al., Phys.Rev.Lett.42, 749 (1979)

23) TASSO Collaboration, R.Brandelik et al., Phys.Lett.92B, 199 (1980)

24) TASSO Collaboration (presented by P.L.Woodworth), Proceedings of European Physical Society International Conference on High Energy Physics, Lisbon, July 9-15, 1981

25) MARK II Collaboration (presented by J.Dorfan) following presentation in these Proceedings (1981)

26) P.Duinker, rapporteur talk, Proceedings of the European Physical Society International Conference on High Energy Physics, Lisbon, July 9-15 , 1981

27) TASSO Collaboration (presented by Sau Lan Wu), Proceedings of the XXth International Conference on High Energy Physics, Madison, Wisconsin, USA, July 17-23, 1980

28) TASSO Collaboration, R. Brandelik et al., Phys. Lett. 100B, 357 (1981)

29) JADE Collaboration, private communication

30) JADE Collaboration, W.Bartel et al., DESY Report 81/025 (1981) (to be published)

31) J.C.Pati and Salam, Nucl.Phys. B 144, 445 (1978)

32) CELLO Collaboration, Contribution to the European Physical Society International Conference on High Energy Physics, Lisbon, July 9-15, 1981

33) R. Marshall, rapporteur talk, European Physical Society International Conferences on High Energy Physics, Lisbon, July 9-15, 1981

34) For definition of oblateness, see D.P.Barber et al., Phys.Rev.Lett. 43, 830 (1979)

35) MARK J Collaboration, D.P.Barber et al., MIT-L.N.S. Report 115 (1981)

36) G.Hanson et al., Phys.Rev.Lett. 35, 1609 (1975)

37) L.Clavelli, Phys.Lett. 85B, 111 (1979)
L.Clavelli and D.Wyler, Phys. Lett. 103B 383 (1981)

38) PLUTO Collaboration, Ch.Berger et al., (to be published)

39) A.V.Smilga, Nucl.Phys. B 161, 449 (1979)

40) B.H.Wiik, Proceedings of the International Neutrino Conference, Bergen, Norway, 18-22 June 1979, p. 113
P.Söding, Proceedings of the European Physical Society International Conference on High Energy Physics, Geneva, Switzerland, 27 June - 4 July 1979, p. 271
41) TASSO Collaboration, R.Brandelik et al., Phys.Lett. 86B, 243 (1979)
42) MARK J Collaboration, D.P.Barber et al., Phys.Rev.Lett. 43, 830 (1979)
43) PLUSO Collaboration, Ch.Berger et al., Phys.Lett.86B, 418 (1979)
44) JADE Collaboration, W.Bartel et al., Phys.Lett. 91B, 142 (1980)
45) J.Ellis, N.K.Gaillard and G.G.Ross,Nucl.Phys. B111, 253 (1976)
46) TASSO Collaboration, R.Brandelik et al., Phys.Lett. 97B, 453 (1980) and W.Braunschweig, Rapporteur talk, 1981, International Symposium on Lepton and Photon Interactions at High Energies, Bonn, August 24-29, 1981
47) J.Ellis and I.Karliner, Nucl.Phys. B148, 141 (1979)
48) PLUTO Collaboration, private communication
49) PLUTO Collaboration, Ch.Berger et al., Phys.Lett. 97B, 459 (1980)
50) Sau Lan Wu, Proceedings of the Arctic School of Physics, Äkäslompolo, Lapland, Finland (1980)
DESY Report 81/003, January 1981, section 4.3.5
51) JADE Collaboration, to be published
52) JADE Collaboration, Phys.Lett. 101B, 129 (1981)
53) Sau Lan Wu and G.Zobernig, Z.Phys. C2, 107 (1979)
54) TASSO Collaboration, R.Brandelik et al., Phys.Lett. 97B, 448 (1980)
55) D.L.Burke et al., Phys.Lett. 103B, 153 (1981)
56) CELLO Collaboration, contributed paper to the European Physical Society International Conference on High Energy Physics, Lisbon, July 9-15, 1981
57) J.Layssac and F.M.Renard, PM 81/5, Montpellier Report, May 1981

58) H.Goldberg and T.Weiler, Phys.Lett. 102B, 63 (1981)
59) S.M. Berman, J.D. Bjorken and J.B. Kogut, Phys.Rev. D4, 3388 (1971)
60) S.J. Bordsky, T. DeGrand, J. Gunion and J. Weis, Phys. Rev. D19, 1418 (1979) and Phys.Rev.Lett. 41, 672 (1978)
61) TASSO Collaboration, R.Brandelik et al., DESY Report 81-053 (1981)
62) JADE Collaboration, W.Bartel et al., DESY Report 81/048 (1981)
63) W.Wagner, Rapporteur talk, Proceedings of the XXth International Conference on High Energy Physics, Madison, Wisconsin, USA, July 17-23, 1980
64) Stan Brodsky, private communication
65) PLUTO Collaboration, Ch.Berger et al., (to be published)
66) E.Witten, Nucl.Phys. B120, 189 (1977)
67) Ch.Llewellyn Smith, Phys.Lett. 79B, 83 (1978)
68) W.R.Frazer and J.F.Gunion, Phys.Rev. D20, 147 (1979)
69) W.A.Bardeen and A.J.Buras, Phys.Rev. D20, 166 (1979)
70) D.W.Duke and J.F.Owens, Phys.Rev. D22, 2280 (1980)
71) C.Peterson, T.F.Walsh and P.M.Zerwas, Nucl.Phys.B 174, 424 (1980)
72) A.J.Buras and D.W.Duke, unpublished
73) S.L.Glashow, Nucl.Phys. 22, 579 (1961)
74) S.Weinberg, Phys.Rev.Lett. 19, 1264 (1967); Phys. Rev. D5, 1412 (1972)
75) A. Salam, Proceedings of the Eighth Nobel Symposium, May 1968, ed. N. Svartholm (Wiley, 1968), p. 367
76) MARK J Collaboration, D.P.Barber et al., Phys.Rev.Lett. 46, 1663 (1981)
77) JADE Collaboration, W.Bartel et al., Phys.Lett. 101B, 361 (1981)
78) J.G.Branson, Rapporteur talk, 1981 International Symposium on Lepton and Photon Interactions at High Energies, Bonn, August 24-29, 1981